iScience

CellPress
OPEN ACCESS

Article

Hypoxia-induced loss of SRSF2-dependent DNA methylation promotes CTCF-mediated alternative splicing of VEGFA in breast cancer

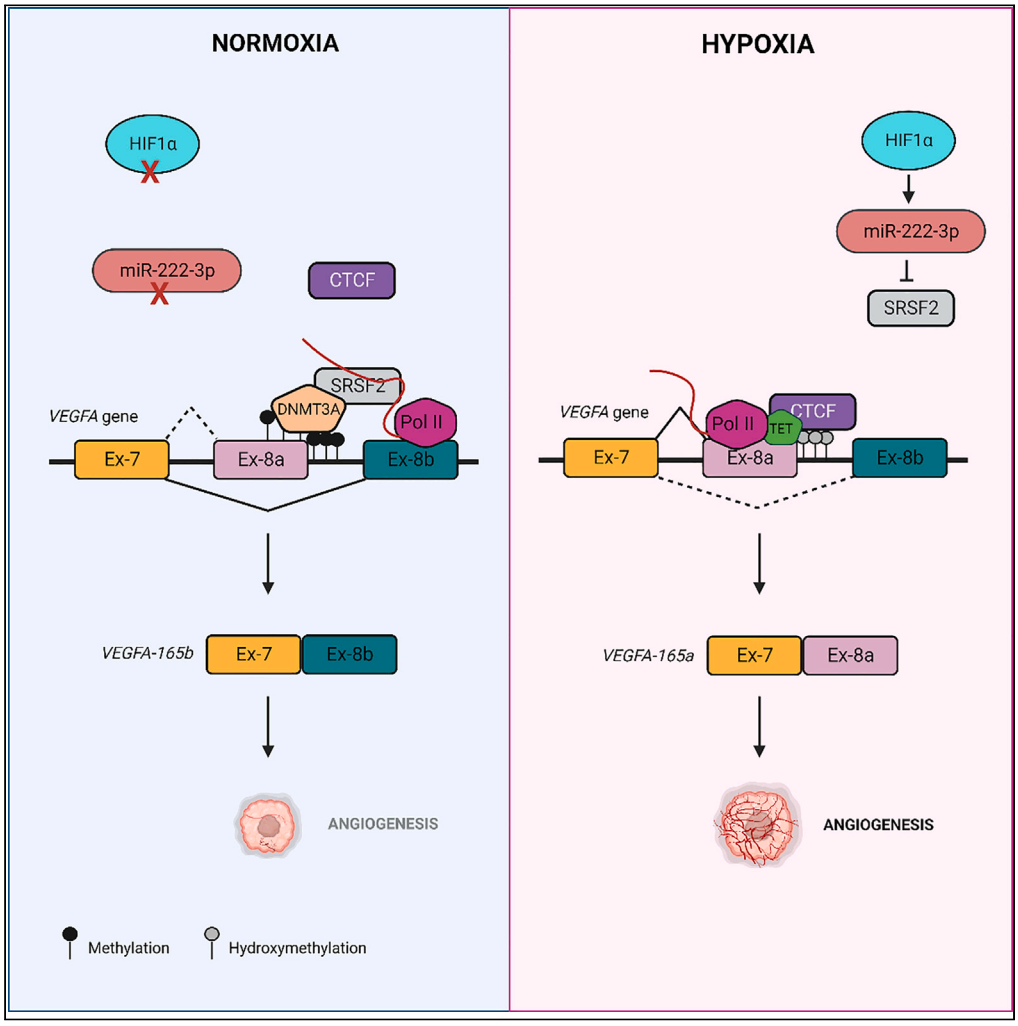

Pooja Yadav, Anchala Pandey, Parik Kakani, Srinivas Abhishek Mutnuru, Atul Samaiya, Jharna Mishra, Sanjeev Shukla

sanjeevs@iiserb.ac.in

Highlights

VEGFA-165 undergoes splicing switch from anti- to pro-angiogenic isoform in hypoxia

HIF1α/miR-222-3p/SRSF2 axis mediates VEGFA-165 splicing

VEGFA-165 splicing is epigenetically regulated by CTCF and DNA methylation

The cross-talk between SRSF2 and DNA methylation controls VEGFA-165 splicing switch

Yadav et al., iScience 26, 106804
June 16, 2023
https://doi.org/10.1016/j.isci.2023.106804

iScience

CellPress
OPEN ACCESS

Article

Hypoxia-induced loss of SRSF2-dependent DNA methylation promotes CTCF-mediated alternative splicing of VEGFA in breast cancer

Pooja Yadav,[1] Anchala Pandey,[1] Parik Kakani,[1] Srinivas Abhishek Mutnuru,[1] Atul Samaiya,[2] Jharna Mishra,[3,4] and Sanjeev Shukla[1,5,*]

SUMMARY

Alternative splicing of vascular endothelial growth factor A (VEGFA) generates numerous isoforms with unique roles in tumor angiogenesis, and investigating the underlying mechanism during hypoxia necessitates diligent pursuance. Our research systematically demonstrated that the splicing factor SRSF2 causes the inclusion of exon-8b, leading to the formation of the anti-angiogenic VEGFA-165b isoform under normoxic conditions. Additionally, SRSF2 interacts with DNMT3A and maintains methylation on exon-8a, inhibiting CCCTC-binding factor (CTCF) recruitment and RNA polymerase II (pol II) occupancy, causing exon-8a exclusion and decreased expression of pro-angiogenic VEGFA-165a. Conversely, SRSF2 is downregulated by HIF1α-induced *miR-222-3p* under hypoxic conditions, which prevents exon-8b inclusion and reduces VEGFA-165b expression. Furthermore, reduced SRSF2 under hypoxia promotes hydroxymethylation on exon-8a, increasing CTCF recruitment, pol II occupancy, exon-8a inclusion, and VEGFA-165a expression. Overall, our findings unveil a specialized dual mechanism of VEGFA-165 alternative splicing, instrumented by the cross-talk between SRSF2 and CTCF, which promotes angiogenesis under hypoxic conditions.

INTRODUCTION

Breast cancer, a solid tumor, is the leading cause of cancer-related death in females.[1] Hypoxia, a commonly recognized feature of solid tumors, is a negative prognostic factor responsible for poor response to treatment and survival in cancer patients.[2] The regions of breast tumors that experience hypoxic stress due to the unavailability of proper vasculature significantly alter several pathways, such as epithelial to mesenchymal transition (EMT), angiogenesis, autophagy, and metabolism, for their survival.[3–5] Angiogenesis, which is crucial for tumor growth and metastasis, requires a balance between pro-angiogenic and anti-angiogenic factors.[6] Therefore, deciphering the mechanism behind angiogenesis regulation in hypoxic tumors is necessary to comprehend the molecular pathways involved in the production of both pro-angiogenic and anti-angiogenic factors. While prior research has explored the impact of hypoxia on angiogenesis,[7] this study represents, to the best of our knowledge, the initial investigation into the intricate mechanism of hypoxia-mediated regulation of vascular endothelial growth factor A (VEGFA) alternative splicing, leading to the differential production of pro-angiogenic and anti-angiogenic isoforms.

VEGFA is a crucial growth factor essential for the development of new blood vessels through angiogenesis. It is secreted along with other growth factors and cytokines, such as fibroblast growth factor (FGF), tumor necrosis factor-alpha (TNF-α), and transforming growth factor-β (TGF-β), during angiogenesis.[8,9] The production of VEGFA is regulated by hypoxia inducible factor α (HIF1α), a protein that plays a vital role in the regulation of angiogenesis in both pathological and physiological contexts. These isoforms are classified as either pro-angiogenic or anti-angiogenic based on the selection of proximal or distal splice sites at exon-8, respectively.[10] Despite existing knowledge about VEGFA's alternative splicing, its mechanism of action under hypoxia remains to be fully understood. As such, further investigation is necessary to gain insights into the regulation of angiogenesis in various physiological and pathological conditions.

[1]Department of Biological Sciences, Indian Institute of Science Education and Research, Bhopal, Madhya Pradesh 462066, India

[2]Department of Surgical Oncology, BH, Bhopal, Madhya Pradesh 462016, India

[3]Department of Pathology, Bansal Hospital (BH), Bhopal, Madhya Pradesh 462016, India

[4]Present address: Neuberg Supratech Kotgirwar Diagnostic, Bhopal

[5]Lead contact

*Correspondence: sanjeevs@iiserb.ac.in

https://doi.org/10.1016/j.isci.2023.106804

Our study has disclosed the mechanism of regulation for the alternative splicing of VEGFA in breast cancer cells under hypoxic conditions. Our findings indicate that the expression of the pro-angiogenic VEGFA-165a isoform, which includes exons 1–5, 7, and 8a, is elevated under hypoxia, while the expression of the anti-angiogenic VEGFA-165b isoform, which includes exons 1–5, 7, and 8b, is reduced.

Through our research, we discovered that a splicing factor called serine and arginine rich splicing factor 2 (SRSF2) plays a key role in the inclusion of exon-8b, leading to the formation of the anti-angiogenic VEGFA-165b isoform under normal oxygen levels. Specifically, we found that SRSF2 under normal oxygen levels facilitates DNA methyltransferase 3A (DNMT3A)-mediated DNA methylation of exon-8a, decreasing CCCTC-binding factor (CTCF) recruitment and polymerase II (pol II) occupancy and consequently leading to the exclusion of exon-8a and the formation of the anti-angiogenic VEGFA-165b isoform. Mechanistically, we also observed that under hypoxia, there is an increase in the expression of a microRNA called *miR-222-3p*, which targets SRSF2, leading to its decreased expression. This decrease in SRSF2 expression results in the exclusion of exon-8b and correlates with an increase in 5-hydroxymethylation at exon-8a. This increased hydroxymethylation aids in the recruitment of CTCF and causes increased pol II occupancy, ultimately leading to the inclusion of exon-8a and the formation of the pro-angiogenic VEGFA-165a isoform.

In summary, our research has uncovered a previously unknown regulatory mechanism that governs the alternative splicing of VEGFA during hypoxia. The study demonstrated that *miR-222-3p* targeting SRSF2 leads to changes in the inclusion or exclusion of exons 8a and 8b, resulting in the formation of either pro-angiogenic or anti-angiogenic isoforms. Additionally, our findings suggest that SRSF2 plays a crucial role in this process through its interaction with CTCF, underscoring the complexity of VEGFA regulation under hypoxia and the importance of further investigating the underlying mechanisms. Collectively, our findings unmask hypoxia-driven regulation of SRSF2 by *miR-222-3p* and uncover a unique mechanism of VEGFA-165 alternative splicing regulation, involving the interplay between SRSF2 and CTCF.

RESULTS

Hypoxia-induced preferential inclusion of exon-8a over exon-8b leads to the accumulation of VEGFA-165a isoform

Tumor cells under hypoxic stress increase angiogenesis to promote their survival and progression in a challenging microenvironment. The expression of various isoforms of VEGFA, a key regulator of angiogenesis, generated through alternative splicing, is not well understood under hypoxic conditions.[11,12] To investigate this, we analyzed existing human transcriptome array 2.0 (HTA 2.0) microarray data of the breast cancer cell line MCF7 under both normoxic and hypoxic conditions (GSE147516).[13] Our splicing index analysis against exon-specific junctions (exon-6b/7a, *VEGFA-206*; exon-5/6a, *VEGFA-189*; exon-5/7a, *VEGFA-165*) revealed significant inclusion of exon-5/7a under hypoxia, corresponding to the *VEGFA-165* isoform, while no other isoform-specific junctions showed significant upregulation or change under normoxic versus hypoxic conditions (Figure S1A). Similar results were found when splicing index analysis was performed for *VEGFA*-specific isoforms in triple-negative breast cancer patients classified as normoxic or hypoxic (GSE76250)[14] (Figure S1B). Additionally, splicing index analysis from the same datasets GSE147516 and GSE76250 of the *VEGFA* exon-7b/8a junction showed significant inclusion ($p = 0.0057$ and $p = 0.0005$, respectively), indicating increased expression of the *VEGFA-165a* isoform in hypoxic compared to normoxic conditions (Figure S1C). The alternative splicing of *VEGFA-165* is shown in Figure 1A. Semi-quantitative PCR was performed for *VEGFA-165a* and *VEGFA-165b* transcripts; the fragments were then gel extracted and sequence confirmed by Sanger sequencing. The chromatograms for *VEGFA-165a* and *VEGFA-165b* are provided in Figure 1B.

We next utilized the RJunBase software to analyze RNA sequencing data and identify the presence of *VEGFA* exon-7/8a and exon-7/8b junctions, which correspond to the *VEGFA-165a* and *VEGFA-165b* transcripts, respectively.[15] Our findings indicated that the *VEGFA* exon-7/8a junction was upregulated, while the exon-7/8b junction was downregulated in tumor breast cancer samples compared to normal samples (Figure S1D). These results were consistent with changes in protein expression of VEGFA-165a and VEGFA-165b observed in MCF7 and HCC1806 cells treated under normoxic and hypoxic conditions (Figures 1C and 1D). To further confirm these results, we employed a dual chromatic VEGFA minigene strategy that involves cloning exon-7, intron-7, exon-8a, and exon-8b of the *VEGFA* gene into a mCherry-N1 vector. The minigene was constructed so that enhanced green fluorescence protein (eGFP) is expressed when exon-8a is included and mCherry is expressed when exon-8b is included. We utilized the *VEGFA* dual chromatic

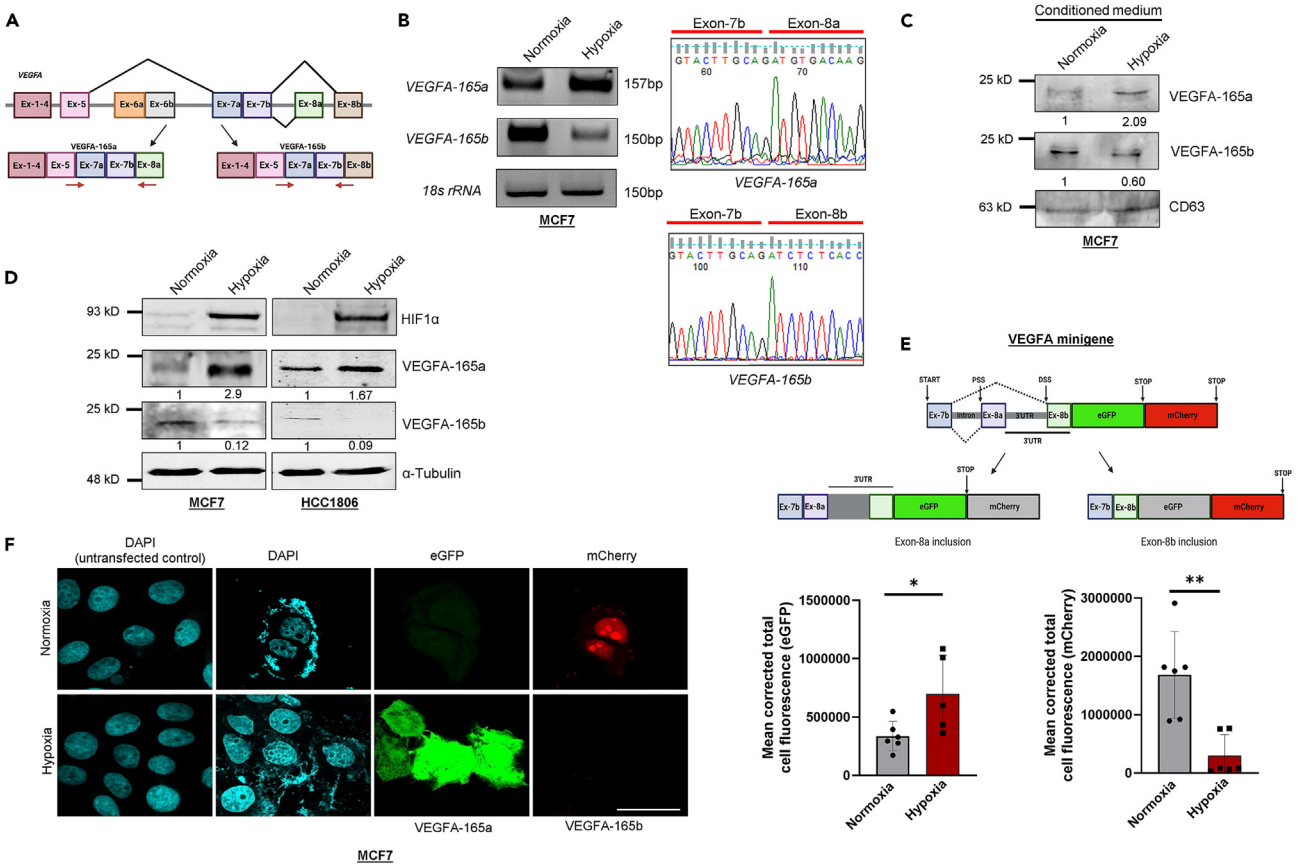

Figure 1. Hypoxia promotes VEGFA exon-8a inclusion and exon-8b exclusion in breast cancer cells

(A) Schematic of VEGFA-165 splicing demonstrating the mutually exclusive event with inclusion of either exon-8b or exon-8a giving rise to VEGFA-165b and VEGFA-165a, respectively.

(B) Semi-quantitative RT-PCR for VEGFA-165a and 165b in MCF7 cells treated under normoxia and hypoxia and the results of Sanger sequencing of the VEGFA-165a and VEGFA-165b isoforms purified from corresponding gels.

(C) Immunoblot for VEGFA-165a and VEGFA-165b with CD63 as loading control in conditioned medium of normoxia- and hypoxia-treated MCF7 cells.

(D) Immunoblot for HIF1α, VEGFA-165a, VEGFA-165b, and α-Tubulin (loading control) under normoxic and hypoxic conditions in MCF7 and HCC1806 cells.

(E) Schematic of VEGFA minigene reporter used, which accommodates exon-7, intron-7, exon-8a, and exon-8b without stop codon. The reporter is designed so that eGFP will be synthesized on exon-8a inclusion and mCherry will be synthesized on exon-8b inclusion.

(F) Confocal microscopy and quantification of VEGFA minigene transfected cells in normoxic and hypoxic conditions. Images are quantified using ImageJ software for mean corrected total cell fluorescence. Scale bar = 20 μm. Statistical significance was determined using unpaired Student's *t* test (*p < 0.05, **p < 0.01, ***p < 0.001, and ****p < 0.0001, while a lack of significance is represented by "ns" for p > 0.05). Error bars show mean values ±SD (n = 3 unless otherwise specified).

minigene construct and detected an upsurge in eGFP expression, indicating an increased incorporation of exon-8a and the production of the pro-angiogenic VEGFA-165a isoform in hypoxic conditions compared to normoxic conditions. Furthermore, a 4′,6-diamidino-2-phenylindole (DAPI) image of untransfected cell nuclei is presented to establish that the extracellular DAPI staining is resulted from transfected DNA and is not mycoplasma contamination (Figures 1E and 1F).

Silencing SRSF2 reduced VEGFA-165b expression under normoxic condition

Having demonstrated alterations in VEGFA-165 splice isoforms' expression under hypoxic conditions in the previous section, we proceeded to investigate the underlying mechanism by exploring the role of splicing factors in regulating VEGFA-165 splicing. We used SFmap, a web-based tool for predicting splicing factors, and identified various splicing factors that bind nearby to VEGFA exon-8.[10,16] We then examined the expression of the identified splicing factors in MCF7 and HCC1806 cells under hypoxic and normoxic conditions using HTA 2.0 microarray data. Our analysis revealed a significant decrease in *SRSF2* expression under hypoxic condition (Figure S2A); the binding site for SRSF2 was identified in the untranslated region

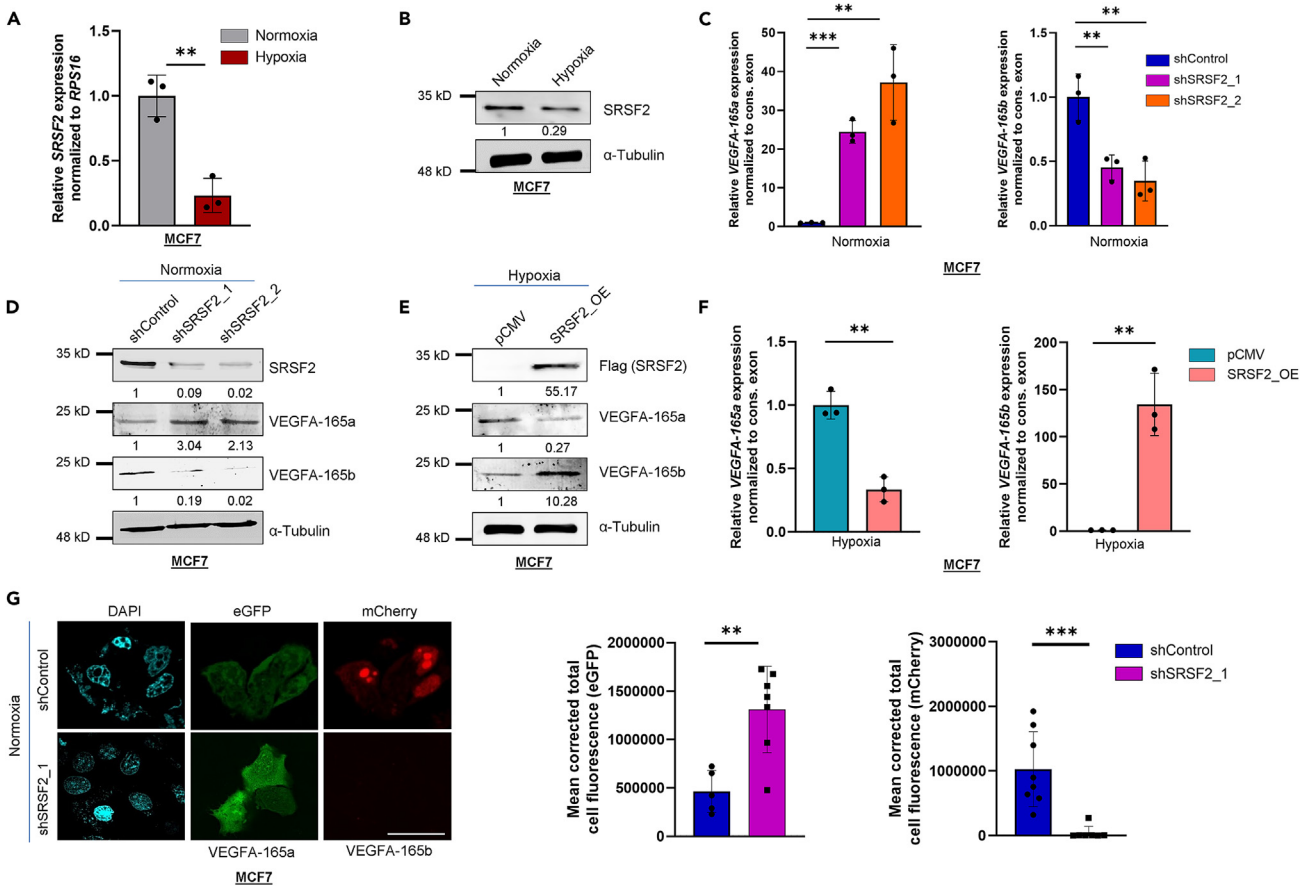

Figure 2. Decrease in VEGFA-165b isoform in the absence of SRSF2 under hypoxic condition in breast cancer cells

(A) qRT-PCR of SRSF2 under hypoxic versus normoxic conditions in MCF7 cells.

(B) Immunoblot of SRSF2 under hypoxic versus normoxic conditions in MCF7 cells.

(C) qRT-PCR of VEGFA-165a and VEGFA-165b isoforms after SRSF2 knockdown under normoxic condition in MCF7 cells.

(D) Immunoblot of SRSF2, VEGFA-165a, and VEGFA-165b isoforms after SRSF2 knockdown under normoxic condition in MCF7 cells.

(E) Immunoblot of flag (SRSF2), VEGFA-165a, and VEGFA-165b isoforms after SRSF2 overexpression under hypoxic condition in MCF7 cells.

(F) qRT-PCR of VEGFA-165a and VEGFA-165b isoforms after SRSF2 overexpression under hypoxic condition in MCF7 cells.

(G) Confocal microscopy and quantification of VEGFA minigene transfected cells in SRSF2 knockdown and control condition under normoxic condition. Scale bar = 20 μm. Statistical significance was determined using unpaired Student's *t* test (*$p < 0.05$, **$p < 0.01$, ***$p < 0.001$, and ****$p < 0.0001$, while a lack of significance is represented by "ns" for $p > 0.05$). Error bars show mean values ±SD (n = 3 unless otherwise specified).

between VEGFA exon-8a and exon-8b. We further confirmed this finding by observing a decrease in SRSF2 expression at both the mRNA and protein levels in MCF7 and HCC1806 cell lines after exposure to hypoxia (Figures 2A, 2B, S2B, and S2C). To investigate the involvement of SRSF2 in VEGFA-165 splicing, we performed short hairpin RNA (shRNA)-mediated knockdown of *SRSF2* under normoxic conditions. We observed that SRSF2 depletion resulted in an increase in the expression of the pro-angiogenic VEGFA-165a isoform and a decrease in the expression of the anti-angiogenic VEGFA-165b isoform in both MCF7 and HCC1806 cells (Figures 2C, 2D, S2D, and S2E). Furthermore, we also confirmed these findings by ectopically expressing SRSF2 under hypoxia and observing a decrease in VEGFA-165a and an increase in VEGFA-165b expression in both the cell lines (Figures 2E, 2F, S2F, and S2G).

To further verify the involvement of SRSF2 in VEGFA-165 splicing, we conducted the VEGFA minigene assay in *SRSF2* knockdown and control MCF7 cells. Our findings demonstrated that the downregulation of SRSF2 resulted in the inclusion of exon-8a, which was evident by increased eGFP expression (Figure 2G). Taken together, these outcomes suggest that the decrease in SRSF2 expression under hypoxia is critical for the inclusion of exon-8a in the VEGFA-165a transcript and the exclusion of exon-8b in VEGFA-165b transcript, thereby promoting angiogenesis.

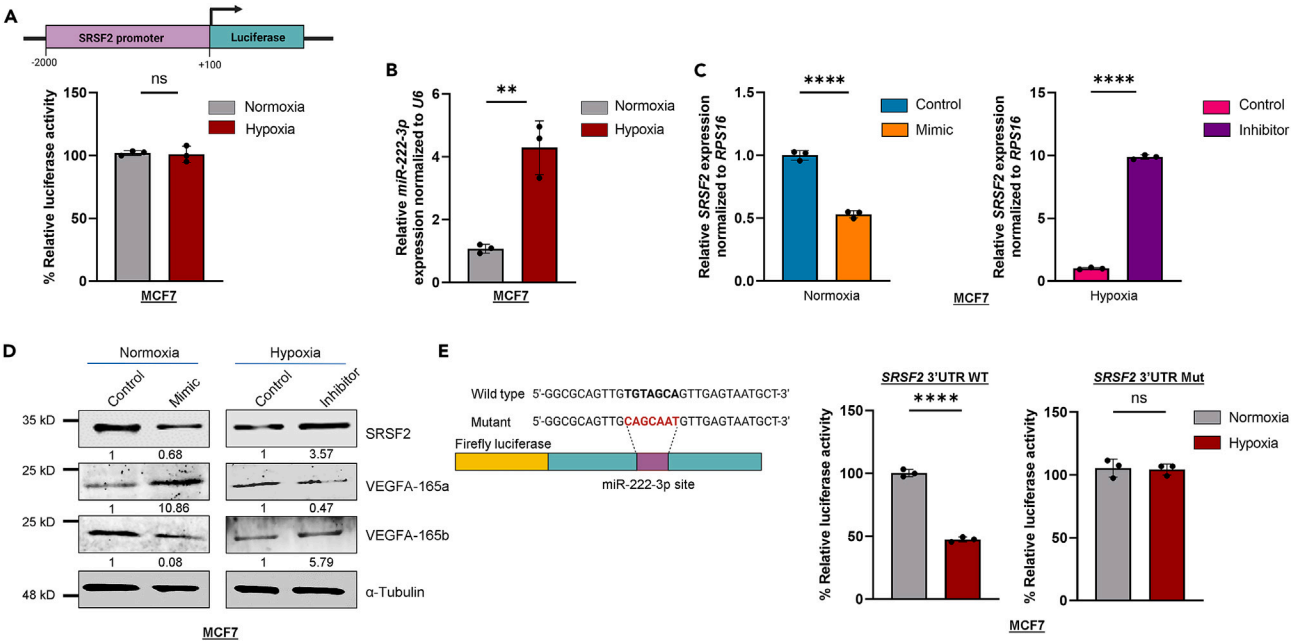

Figure 3. miR-222–3p downregulates SRSF2 expression post-transcriptionally under hypoxic condition

(A) Dual-luciferase assay with SRSF2 promoter under normoxic versus hypoxic conditions in MCF7 cells. The relative luciferase values are shown as mean ± SD.

(B) qRT-PCR of miR-222–3p under normoxic versus hypoxic conditions in MCF7 cells.

(C) qRT-PCR of SRSF2 on miR-222-3p mimic and inhibitor transfection under normoxic and hypoxic conditions, respectively, in MCF7 cells with their negative controls.

(D) Immunoblot of SRSF2, VEGFA-165a, and VEGFA-165b after miR-222–3p mimic and inhibitor transfection under normoxic and hypoxic condition, respectively, in MCF7 cells with their negative controls.

(E) Schematic showing wild-type and mutant miR-222–3p binding site utilized for dual-luciferase assay. Dual-luciferase assay with wild-type and mutant miR-222–3p binding site on SRSF2 3′UTR under normoxic versus hypoxic conditions represented as N and H, respectively, in MCF7 cells. 3′UTR- 3′ untranslated region, miR-microRNA, and mimic negative control and inhibitor negative control are both labeled Control. Statistical significance was determined using unpaired Student's *t* test (*p < 0.05, **p < 0.01, ***p < 0.001, and ****p < 0.0001, while a lack of significance is represented by "ns" for p > 0.05). Error bars show mean values ±SD (n = 3 unless otherwise specified).

miR-222-3p inhibits *SRSF2* expression post-transcriptionally under hypoxia via direct interaction with *SRSF2* 3′UTR

To comprehend the mechanism underlying the inhibition of SRSF2 under hypoxia, we analyzed the transcriptional regulation of the *SRSF2* promoter using a dual-luciferase reporter assay. Our findings revealed no significant alteration in luciferase activity in normoxic versus hypoxic conditions, implying that the downregulation of SRSF2 under hypoxia is not regulated transcriptionally (Figures 3A and S3A). To corroborate this outcome, we also employed a luciferase construct containing four copies of the suppressor of mothers against decapentaplegic (SMAD) binding element upstream of the luciferase reporter gene as a positive control (Figure S3B).

After noting the absence of transcriptional regulation, our focus shifted to investigating alternative regulatory mechanisms involved in the downregulation of SRSF2 during hypoxia. Recent findings suggest that microRNAs (miRNAs) play an important role in post-transcriptional regulation of alternative splicing by silencing splicing regulators.[17] Furthermore, miRNAs may be differentially expressed under hypoxia due to the direct or indirect regulation by HIF1α or other transcription factors.[18,19]

To understand the impact of miRNAs on the regulation of SRSF2 expression and its effect on VEGFA-165 splicing, we performed further investigation. Bioinformatics analysis using TargetScan 7.2 revealed several miRNAs (*miR-193-3p*, *miR-200bc-3p*, *miR-429*, *miR-133a-3p*, *miR-183-5p*, *miR-338-3p*, *miR-130-3p*, *miR-301-3p*, *miR-454-3p*, and *miR-222-3p*) that bind to the *SRSF2* 3′UTR region. However, only *miR-222-3p* showed an increase in expression among the other miRNAs targeting *SRSF2*, under hypoxia treatment

in HTA 2.0 microarray data (GSE147516). To confirm these results, we quantified the expression of *miR-222-3p* using TaqMan miRNA assays and found elevated expression of *miR-222-3p* in both MCF7 and HCC1806 under hypoxia (Figures 3B and S3C).

In order to confirm the involvement of *miR-222-3p* in the downregulation of SRSF2 during hypoxia, we conducted an experimental validation by transfecting MCF7 and HCC1806 cells with *miR-222-3p* mimic and inhibitor, along with controls. The results obtained through qRT-PCR and immunoblotting indicated that the transfection with the *miR-222-3p* mimic caused a reduction in SRSF2 expression compared to the control under normoxia, while transfection with the *miR-222-3p* inhibitor led to an elevation in SRSF2 expression compared to the control under hypoxia (Figures 3C, 3D, S3D, and S3F).

We conducted a dual reporter luciferase assay in MCF7 and HCC1806 cells to confirm the direct regulation of SRSF2 expression by *miR-222-3p*. To achieve this, we cloned *miR-222-3p* seed pairing sites (wild-type and mutated) and the immediate surrounding sequences in the *SRSF2* 3′UTR downstream of the luciferase open reading frame of the pMIR-REPORT vector. The results indicated a decrease in luciferase activity when transfection was performed with the construct containing wild-type binding site in normoxic versus hypoxic conditions, while no change in luciferase activity was observed when transfection was performed with a construct containing the mutated *miR-222-3p* binding site on the *SRSF2* 3′UTR (Figures 3E and S3E).

The expression of VEGFA-165 isoforms was affected by transfecting *miR-222-3p* mimic and inhibitor into MCF7 and HCC1806 cells. The results, as shown in Figures 3D, S3F, S3G, and S3H, revealed that the *miR-222-3p* mimic caused an increase in VEGFA-165a expression, while the *miR-222-3p* inhibitor suppressed VEGFA-165a expression. Conversely, the *miR-222-3p* mimic suppressed VEGFA-165b expression, while the *miR-222-3p* inhibitor increased its expression, at both mRNA and protein levels in both MCF7 and HCC1806 cells. These findings suggest that hypoxia-induced *miR-222-3p* has a unique role in promoting angiogenesis by suppressing SRSF2, which results in reduced expression of the VEGFA-165b isoform.

HIF1α-mediated *miR-222-3p* upregulation modulates *VEGFA* alternative splicing

Up to this point, we have demonstrated that hypoxia-induced *miR-222-3p* expression modulation plays a role in regulating VEGFA-165 alternative splicing. In order to gain a deeper understanding of this regulation, we investigated the involvement of HIF1α, a transcription factor known to upregulate hypoxia-inducible genes in cancer cells. Our analysis of publicly available HIF1α chromatin immunoprecipitation sequencing (ChIP-seq) data from ChIP-Atlas (https://chip-atlas.org) revealed the presence of HIF1α binding on the *miR-222* promoter (Figure 4A). Consistent with this, our ChIP-qPCR results demonstrated significant enrichment of HIF1α on the *miR-222* promoter compared to the normoxic control (Figures 4B and S4A). Additionally, we conducted shRNA-mediated *HIF1α* knockdown experiments to investigate the effect of HIF1α on *miR-222-3p* expression, which resulted in a significant decrease in *miR-222-3p* expression under hypoxia (Figures 4C and S4B). We also observed that HIF1α depletion caused an increase in VEGFA-165b isoform and a decrease in VEGFA-165a, both at the mRNA and protein levels (Figures 4D, 4E, S4C, and S4D). These results substantiated the role of the HIF1α-*miR-222-3p* axis in regulating VEGFA-165 alternative splicing by suppressing SRSF2 expression. In addition, using a VEGFA minigene system, we demonstrated that HIF1α is necessary for the inclusion of VEGF 165 exon-8a (Figure 4F). Overall, our findings indicate that HIF1α plays a crucial role in promoting angiogenesis under hypoxic condition by directly inducing *miR-222-3p* expression.

Increased hydroxymethylation at the exon-8a region contributes to CTCF recruitment under hypoxic condition

Our research has provided insights into the regulation of VEGFA-165 alternative splicing under hypoxic condition. We have discovered that the HIF1α-*miR-222-3p*-SRSF2 axis mediates the exclusion of exon-8b and generation of VEGFA-165a isoform by reducing the expression of SRSF2 under hypoxia. However, we still needed to understand the mechanism behind VEGFA-165 exon-8a inclusion under hypoxic conditions in the absence of SRSF2.

Recent studies have shown that epigenetic mechanisms, particularly DNA methylation, contribute to the alternative splicing.[20–22] Importantly, the binding of a DNA-binding protein CTCF depends on the presence or absence of 5-methylcytosine (5-mC) marks on the target exon.[23,24] Moreover, hydroxymethylation of cytosine has been demonstrated to facilitate the recruitment of CTCF.[23] Additionally, there is ample

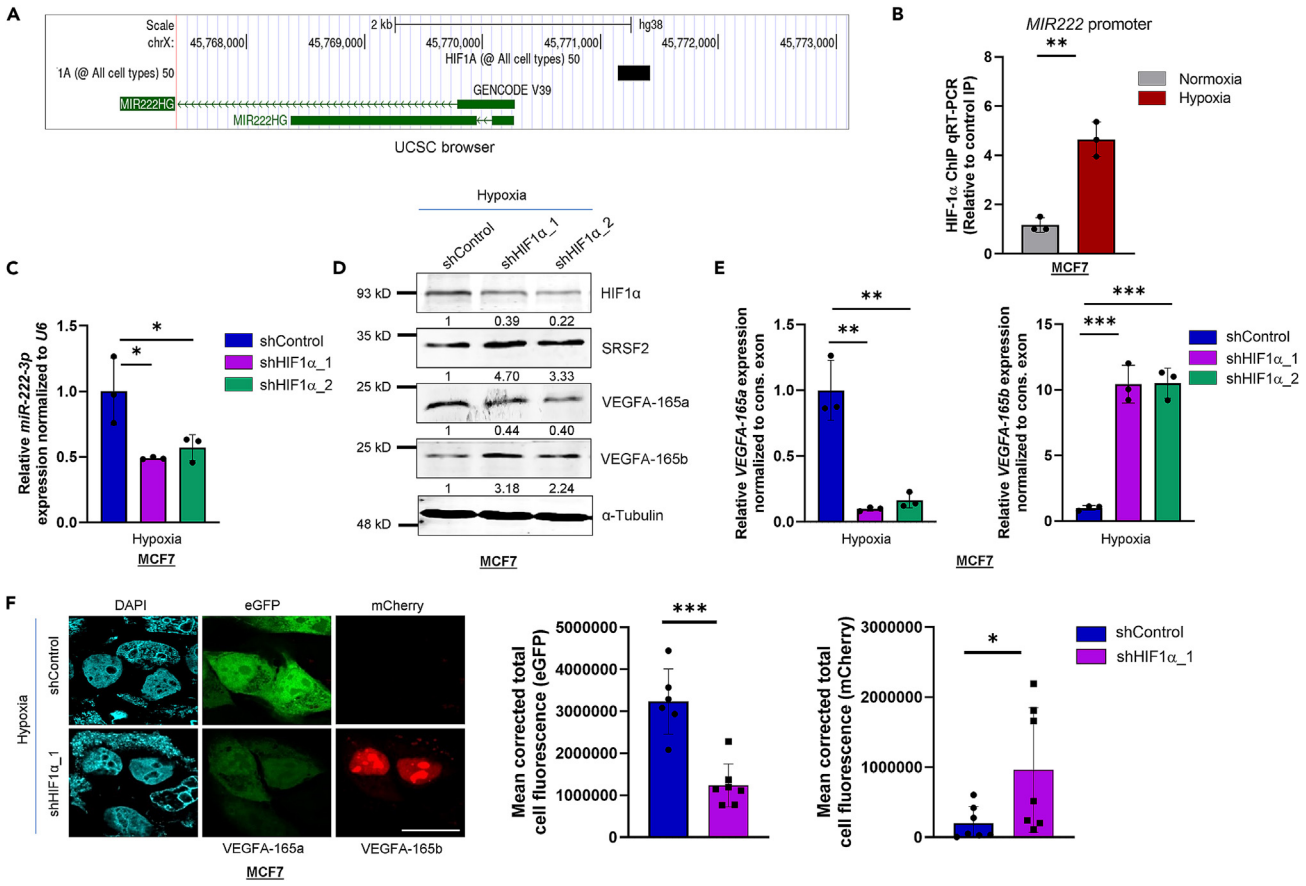

Figure 4. HIF1α regulates VEGFA alternative splicing directly by upregulating miR-222-3p

(A) HIF1α binding site is present on MIR222 promoter.

(B) ChIP qRT-PCR on MIR222 promoter using HIF1α antibody in normoxic versus hypoxic conditions in MCF7 cells. Fold enrichment (HIF1α/IgG) was normalized to input.

(C) qRT-PCR of miR-222-3p after HIF1α knockdown under hypoxic condition in MCF7 cells.

(D) Immunoblot of HIF1α, SRSF2, VEGFA-165a, and VEGFA-165b isoforms after HIF1α knockdown under hypoxic condition in MCF7 cells.

(E) qRT-PCR of VEGFA-165a and VEGFA-165b isoforms after HIF1α knockdown under hypoxic condition in MCF7 cells.

(F) Confocal microscopy and quantification of VEGFA minigene transfected cells in HIF1α knockdown and control condition under hypoxia. Scale bar = 20 μm. Statistical significance was determined using unpaired Student's *t* test (*p < 0.05, **p < 0.01, ***p < 0.001, and ****p < 0.0001, while a lack of significance is represented by "ns" for p > 0.05). Error bars show mean values ±SD (n = 3 unless otherwise specified).

amount of evidence suggesting that the CTCF binding promotes the inclusion of weak upstream exons by mediating local RNA pol II pausing.[22,25,26]

Based on these findings, we hypothesized that CTCF might regulate VEGFA-165 alternative splicing in the absence of SRSF2 under hypoxic condition. Bioinformatics analysis using CIS-BP (http://cisbp.ccbr.utoronto.ca) revealed a putative CTCF binding site on VEGFA exon-8a. To investigate the involvement of DNA methylation and CTCF in VEGFA alternative splicing, we performed Methylated DNA immunoprecipitation (MeDIP) and hydroxymethylated DNA immunoprecipitation (hMeDIP)-qPCR using antibodies against 5-methylcytosine (5-mC) and 5-hydroxymethylcytosine (5-hmC), respectively. We observed a significant decrease in 5-mC and a concomitant increase in 5-hmC levels under hypoxic as compared to normoxic conditions at exon-8a, but no change was observed in methylation status at exon-8b in MCF7 and HCC1806 cells (Figures 5A, 5B, S5A, and S5B).

Next, we performed CTCF and pol II ChIP under normoxic and hypoxic conditions. In line with the reduced methylation and enhanced hydroxymethylation at exon-8a (Figures 5C and S5C), we observed an increased binding of CTCF at exon-8a, which correlated with increased enrichment of pol II at exon-8a in hypoxic

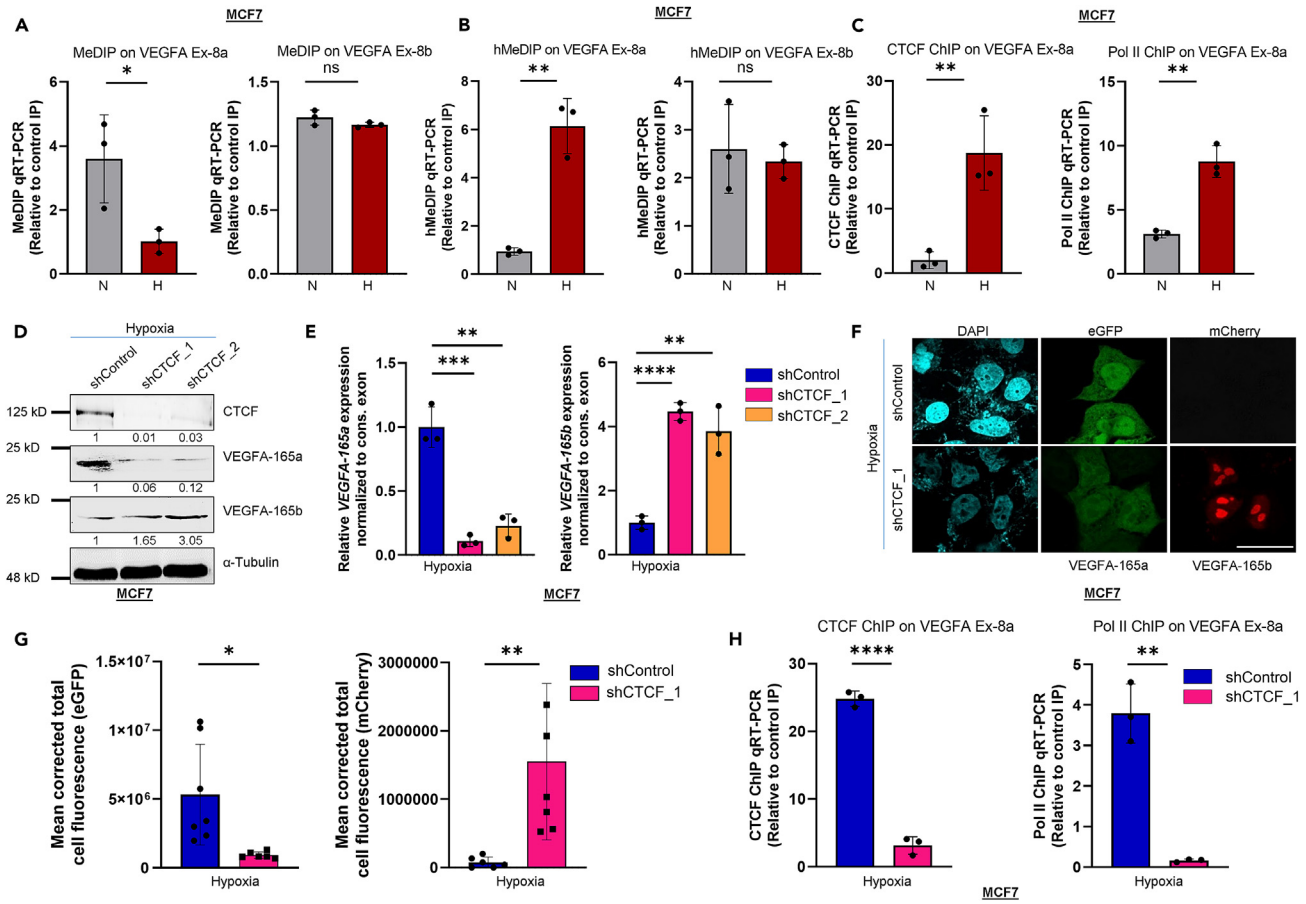

Figure 5. Increased hydroxymethylation under hypoxic conditions contributes to the involvement of CTCF in VEGFA AS

(A and B) qRT-PCR analysis of MeDIP and hMeDIP performed in normoxia versus hypoxia treatment represented as N and H, respectively, in MCF7 cells' genomic DNA using 5-methylcytosine and 5-hydroxymethylcytosine antibody and VEGFA exon-8a and VEGFA exon-8b primers.

(C) ChIP qRT-PCR on VEGFA using CTCF and pol II antibodies in normoxic versus hypoxic conditions in MCF7 cells.

(D) Immunoblot and qRT-PCR analysis of CTCF, VEGFA-165a, and VEGFA-165b isoforms after CTCF knockdown under hypoxic condition in MCF7 cells.

(E) qRT-PCR of VEGFA-165a and VEGFA-165b isoforms after CTCF knockdown under hypoxic condition in MCF7 cells.

(F and G) Confocal microscopy and quantification of VEGFA minigene transfected cells in CTCF knockdown and control condition under hypoxia. Scale bar = 20μm.

(H) ChIP qRT-PCR on VEGFA using CTCF and pol II antibody in control versus CTCF knockdown under hypoxic condition in MCF7 cells. Fold enrichment (CTCF/IgG) and (pol II/IgG) was normalized to input. Statistical significance was determined using unpaired Student's *t* test (*p < 0.05, **p < 0.01, ***p < 0.001, and ****p < 0.0001, while a lack of significance is represented by "ns" for p > 0.05). Error bars show mean values ±SD (n = 3 unless otherwise specified).

compared to normoxic MCF7 cells. To further validate our findings, we performed shRNA-mediated depletion of *CTCF* in MCF7 and HCC1806 cells under hypoxic conditions. Notably, CTCF knockdown resulted in a decrease in VEGFA-165a and increased VEGFA-165b expression at both RNA and protein levels (Figures 5D, 5E, S5D, and S5E).

Next, we conducted minigene analysis and found that the knockdown of *CTCF* in MCF7 cells under hypoxic conditions led to a decrease in eGFP and an increase in mCherry expression. This result indicates a loss of VEGFA-165a isoform compared to control, as shown in Figures 5F and 5G. We also found that under hypoxic conditions, *CTCF* depletion caused a reduction in both CTCF and pol II binding on VEGFA-165 exon-8a but no change at the exon-8b (Figures 5H and S5F–S5H). These results indicate that hypoxia triggers changes in the epigenetic landscape, leading to the recruitment of CTCF at VEGFA-165 exon-8a, causing pol II pause, and facilitating exon-8a inclusion, resulting in the generation of a pro-angiogenic isoform of VEGFA-165a.

The interplay between SRSF2 and CTCF tunes the alternative splicing of VEGFA-165

The findings so far indicate that hypoxia increases the expression of VEGFA-165a by reducing SRSF2 levels and decreasing methylation on exon-8a. This results in the recruitment of CTCF and the pause of pol II. However, changes in expression of VEGFA-165a isoform expression were also observed in *SRSF2* knockdown cells under normal oxygen levels. This prompts further investigation into the role of SRSF2 in VEGFA-165 splicing. According to previous reports, splicing factors can modify epigenetic marks by interacting with epigenetic modifiers.[27–30] Moreover, SRSF2 can modulate H3K27ac levels by associating with the p300/cyclic AMP response element-binding protein (CBP) acyl-transferase complex, acting as an anti-tumor modulator.

To determine the role of SRSF2 in regulating DNA methylation on exon-8 of VEGFA-165, MeDIP-qPCR and hMeDIP-qPCR were performed in *SRSF2* knockdown cells. The results indicated that SRSF2 knockdown causes a decrease in methylation and an increase in hydroxymethylation at exon-8a, indicating its role in regulating methylation and CTCF recruitment at exon-8a (Figures 6A and S6A–S6C). CTCF and pol II ChIP-qPCR were also performed in *SRSF2* knockdown cells, revealing enriched binding of both CTCF and pol II at exon-8a under normal oxygen levels in *SRSF2* knockdown cells compared to control (Figures 6B, S6D, S6E, and S6F). These findings suggest that SRSF2 plays a dual role in VEGFA-165 splicing, not only as a splicing factor involved in the inclusion of exon-8b but also in regulating methylation status at exon-8a and altering CTCF recruitment.

To enhance the comprehension of the alternative splicing of VEGFA-165 under hypoxic conditions, we aimed to investigate the role of ten-eleven translocases (TETs) proteins, which are accountable for the transformation of 5-mC to 5-hmC, following the observed rise in 5-hmC marks at the exon-8a site of *VEGFA*. We performed CTCF ChIP-qPCR analysis while inhibiting TETs using TET inhibitor (TET-i) Bobcat and discovered that CTCF enrichment and hydroxymethylation at exon-8a decreased upon TET inhibition (Figures 6C, S6G, and S6H). This observation implies that, under hypoxia, TETs are vital for transforming 5-mC to 5-hmC, subsequently allowing the binding of CTCF at exon-8a and thereby causing its inclusion.

Our findings thus far suggest that SRSF2 and DNMT3A play crucial roles in regulating VEGFA alternative splicing under normoxic condition by maintaining the methylation status at exon-8a and promoting exon-8b inclusion. Therefore, we hypothesized that SRSF2 might interact with DNMTs under normoxic conditions. Through STRING analysis, we found evidence of direct interaction between SRSF2 and DNMT3A, which we verified through MeDIP and hMeDIP assays and co-immunoprecipitation (coIP) experiments (Figure S6I). To confirm the involvement of DNMT3A in VEGFA alternative splicing, we performed immunoblot analysis of VEGFA isoforms and observed a decrease in VEGFA-165b and an increase in VEGFA-165a in *DNMT3A* knockdown cells under normoxia (Figures 6D and S6J). Our results also demonstrated a decrease in methylation and an increase in hydroxymethylation at exon-8a on *DNMT3A* knockdown, indicating its role in maintaining VEGFA-165b expression under normoxic conditions (Figure 6E). Moreover, our coIP results revealed a direct interaction between DNMT3A and SRSF2 under normoxic conditions, providing additional evidence that this interaction is responsible for exon-8b inclusion under normoxic conditions (Figure 6F).

Clinical validation of hypoxia-induced VEGFA-165 alternative splicing

Our investigation has thoroughly uncovered the mechanism underlying VEGFA-165 alternative splicing in breast cancer cells. The identification of the molecular players involved in VEGFA alternative splicing could have significant clinical implications. To gain a better understanding of the status of these molecular players, we conducted an immunohistochemistry (IHC) analysis on tumor sections obtained from breast cancer patients. The sections were stained with antibodies against VEGFA-165a, VEGFA-165b, and SRSF2, and we used carbonic anhydrase 9 (CAIX) as a marker for hypoxia.[31] Our results revealed that regions of high hypoxia, as indicated by positive CAIX staining, exhibited intense staining for VEGFA-165a and weak staining for SRSF2 and VEGFA-165b. Conversely, regions with low hypoxia, as indicated by negative CAIX staining, showed strong staining for SRSF2 and VEGFA-165b and weak staining for VEGFA-165a. Taken together, our *in vivo* observations corroborate with our *in vitro* results, demonstrating that, under hypoxic conditions, there is a reduction in the level of SRSF2 levels, leading to epigenetic-mediated alternative splicing of the VEGFA gene, which promotes the production of the

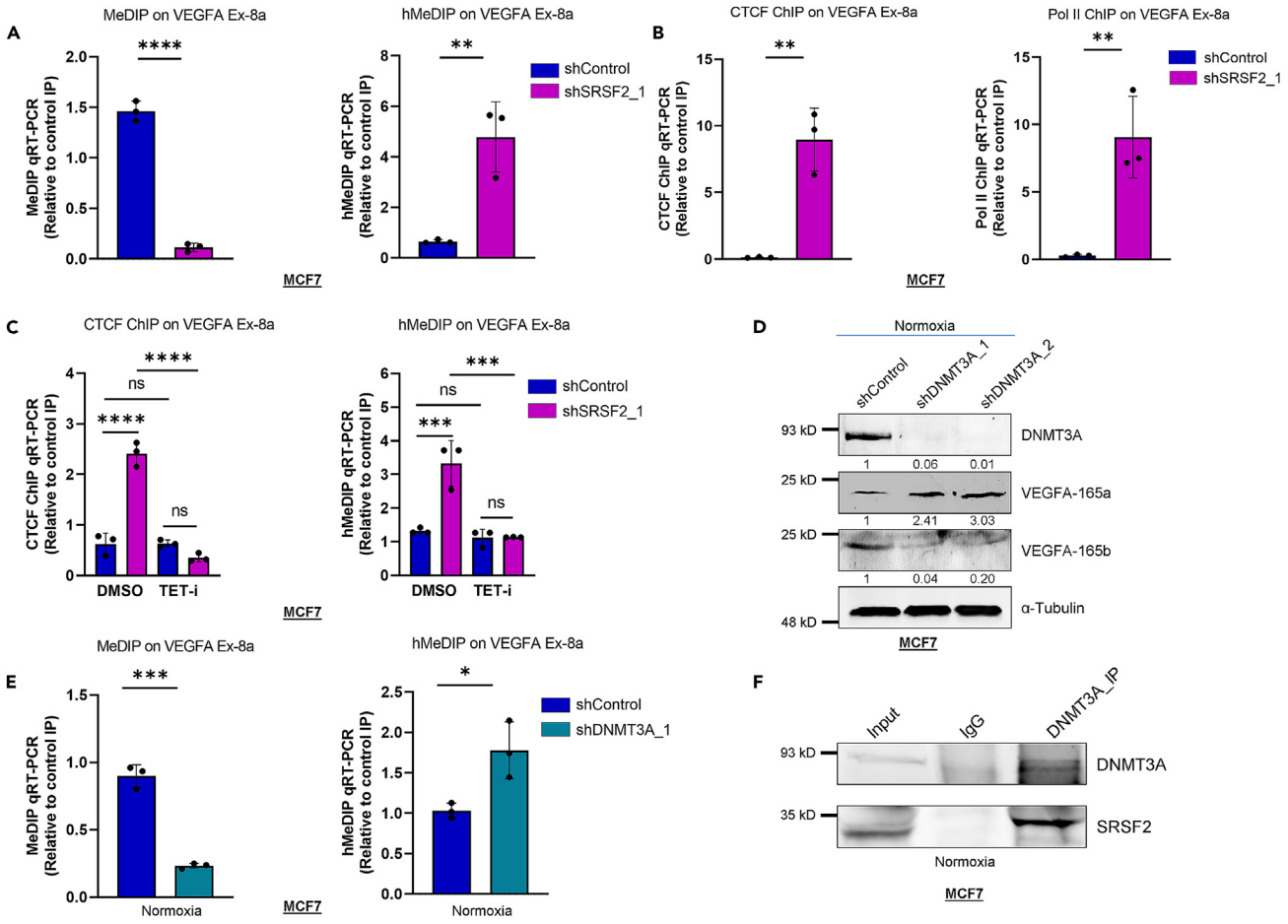

Figure 6. Cross-talk between epigenetic and splicing mechanism for VEGFA splicing

(A) qRT-PCR analysis of MeDIP and hMeDIP performed in control versus SRSF2 knockdown under normoxia in MCF7 cells DNA using 5-methylcytosine and 5-hydroxymethylcytosine antibody and VEGFA exon-8a primers.

(B) ChIP qRT-PCR on VEGFA exon-8a using CTCF and pol II antibody in control versus SRSF2 knockdown MCF7 cells under hypoxic condition.

(C) ChIP and hMeDIP qRT-PCR on VEGFA exon-8a using CTCF and 5-hydroxymethylcytosine antibody respectively in DMSO versus TET inhibitor Bobcat (TET-i) in control and SRSF2 knockdown MCF7 cells under normoxic condition. Fold enrichment (CTCF/IgG) and (5-hydroxymethylcytosine/IgG) was normalized to input.

(D) Immunoblot of DNMT3A, VEGFA-165a, and VEGFA-165b isoforms after DNMT3A knockdown under normoxic condition in MCF7 cells.

(E) qRT-PCR analysis of MeDIP and hMeDIP performed in control versus DNMT3A knockdown under normoxia in MCF7 cells' DNA using 5-methylcytosine and 5-hydroxymethylcytosine antibody and VEGFA exon-8a primers.

(F) DNMT3A and SRSF2 interact endogenously. CoIP was performed with DNMT3A antibody under normoxic condition with IgG as control. The immunoprecipitated samples were analyzed using SRSF2 and DNMT3A antibody by immunoblotting. Statistical significance was determined using unpaired Student's *t* test (*p < 0.05, **p < 0.01, ***p < 0.001, and ****p < 0.0001, while a lack of significance is represented by "ns" for p > 0.05). Error bars show mean values ± SD (n = 3 unless otherwise specified).

pro-angiogenic VEGFA-165a isoform over the anti-angiogenic VEGFA-165b isoform, thus inducing angiogenesis (Figures 7, S7, and S8).

DISCUSSION

Despite recent advancements in breast cancer treatment, it continues to be a leading cause of cancer-related deaths in women.[32] Hypoxia is a significant contributor to breast cancer progression,[33,34] causing alterations in the expression of various genes through alternative splicing, which helps cancer cells survive and evade treatment.[13,35–38] Angiogenesis, the development of new blood vessels, is also a critical aspect of breast cancer progression and is heavily influenced by the expression and alternative splicing of angiogenic genes.[6,39,40]

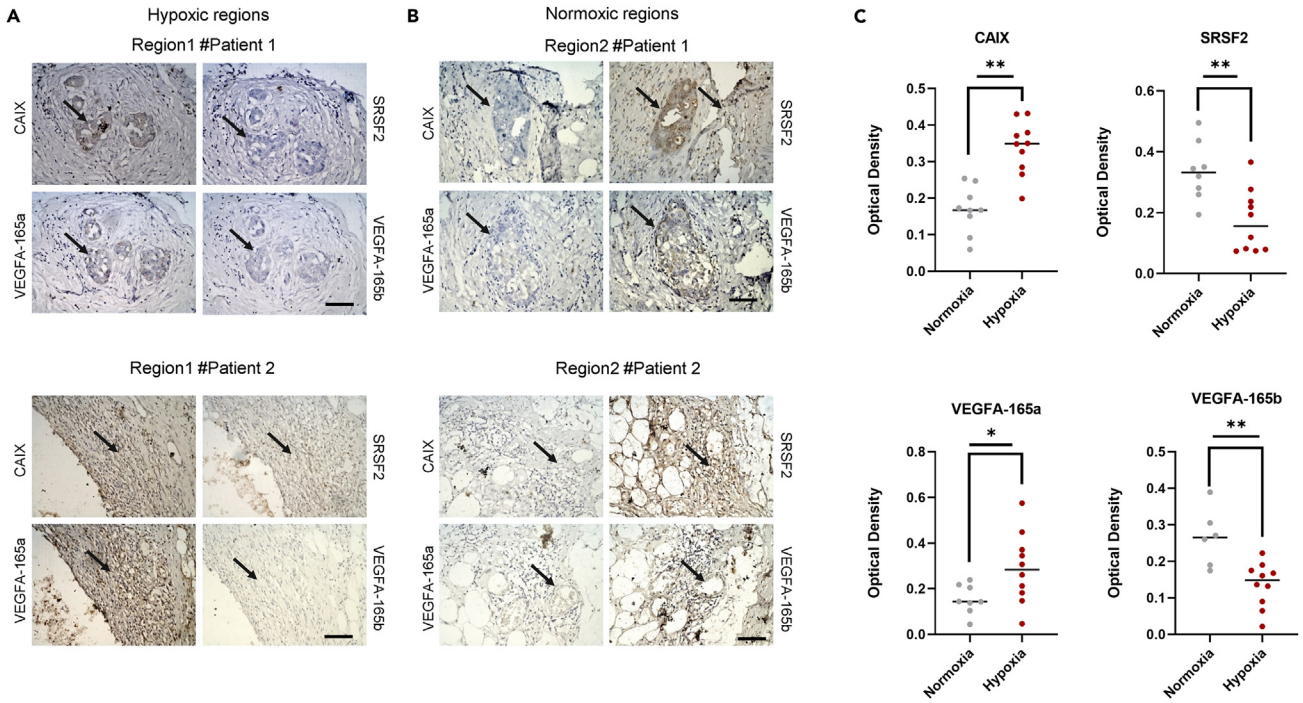

Figure 7. Clinical validation of hypoxia-induced VEGFA alternative splicing

(A) Hypoxic regions of patient 1 and 2. Hypoxic region showed strong immunostaining of CAIX and VEGFA-165a and weak immunostaining of SRSF2 and VEGFA-165b.

(B) Normoxic regions of patient 1 and 2. Normoxic regions showed weak immunostaining of CAIX and VEGFA-165a and strong immunostaining of SRSF2 and VEGFA-165b.

(C) Quantification for CAIX, SRSF2, VEGFA-165a, and VEGFA-165b staining represented as optical density for hypoxic versus normoxic regions of 12 breast cancer patient's samples. Statistical significance was determined using unpaired Student's *t* test (*p < 0.05, **p < 0.01, ***p < 0.001, and ****p < 0.0001, while a lack of significance is represented by "ns" for p > 0.05). Scale bar = 100 μm, Magnification is 40×.

The objective of this study is to gain a better understanding of how hypoxia, via the transcription factor HIF1α, controls the alternative splicing of the angiogenic gene VEGFA in breast cancer cells.

Due to the presence of the hypoxia responsive element (HRE), VEGFA upregulation is widely discussed in the context of different cancers under hypoxic stress.[41] Despite several reports demonstrating alternative splicing of VEGFA, the mechanism behind its alternative splicing under hypoxic condition remains elusive.[10,42,43] VEGFA alternative splicing generates multiple isoforms, with VEGFA-165 being one of the most frequently expressed isoforms.[44] The splicing switch at the C terminus of *VEGFA* transcripts determines the production of two classes of transcripts having opposite functions. Our study discovered that, under hypoxic stress, the *VEGFA-165* transcript undergoes alternative splicing, leading to the inclusion of exon-8a and exclusion of exon-8b, resulting in the production of the pro-angiogenic VEGFA-165a isoform over the anti-angiogenic VEGFA-165b isoform. Several splicing factors, such as SRSF1, SRSF2, and SRSF6, have been identified to be involved in VEGFA splicing; however, the splicing factor regulating VEGFA alternative splicing under hypoxia was unknown.[10,45–47] We observed a significant reduction in SRSF2 expression in breast cancer cells exposed to hypoxic stress. Additionally, SRSF2 expression alteration caused a switch in the expression of VEGFA-165 isoforms at both mRNA and protein levels, establishing it as the splicing factor responsible for VEGFA-165 alternative splicing under hypoxic stress.

MicroRNAs play a crucial role in oncogenesis as regulators of various processes acting either as oncogenes or tumor suppressors.[48] They negatively regulate target gene expression through sequence-specific RNA-RNA interactions with the 3′-UTRs, and their dysregulation is frequently observed under hypoxia.[49] The role of miRNAs in regulating alternative splicing has been previously reported.[50] In this study, we discovered *miR-222-3p* as a previously unknown regulator of VEGFA alternative splicing and angiogenesis, functioning at the interface between VEGFA alternative splicing and SRSF2. Our findings suggested that *miR-222-3p*

acts as a negative regulator, responsible for the decrease in SRSF2 expression under hypoxic conditions. These findings are consistent with the previous work of Liu et al., who have also investigated the role of *miR-222-3p*/SRSF2 in regulating cancer progression under hypoxic conditions. Liu et al. have shown that hypoxia-induced *miR-222-3p* inhibits the expression of SRSF2, resulting in the alternative splicing of methyl-CpG binding domain 2 (MBD2), which activates frizzled class receptor (FZD1) and promotes epithelial to mesenchymal transition and metastasis.[37] Experiments using *miR-222-3p* mimic and inhibitor further demonstrated the involvement of *miR-222-3p* in mediating VEGFA-165 exon-8b exclusion under hypoxic conditions. However, the mechanism behind VEGFA-165 exon-8a inclusion under hypoxia remains unclear. Although miRNAs' involvement in regulating VEGFA expression is extensively documented, this study reveals their impact on VEGFA-165 alternative splicing and its effect on angiogenesis, which has not been previously reported.[51,52] HIF1α, the master regulator of the hypoxic response, activates a significant number of genes that promote tumor growth and malignant progression.[53] We hypothesized that HIF1α might also be involved in orchestrating the VEGFA alternative splicing event. Our bioinformatics analysis revealed the presence of an HRE element in the promoter region of the *miR222* gene, which was also confirmed by HIF1α ChIP-qPCR, indicating that HIF1α transcriptionally regulates *miR-222-3p*. Therefore, this study's findings on the splicing of VEGFA exon-8a/b, which is mediated by *miR-222-3p*/SRSF2 during hypoxia, confirm and build upon the previous report by Liu et al.[37] While the reigning paradigm suggests that HIF1α upregulates the expression of its target genes under hypoxia, our findings show that its control of *miR-222-3p* expression also determines its role in regulating alternative splicing.

Alternative splicing and epigenetics are closely connected in regulating gene expression.[54] Several studies have indicated a bidirectional relationship between epigenetics and RNA processing, particularly the involvement of chromatin in splicing regulation.[55–57] For instance, ALKBH5, a demethyltransferase, has been found to impact the localization of splicing factors such as SRSF2, SRPK1, and ASF/SF2.[58] Tumors use these mechanisms to generate new proteins from pre-mRNA that help them survive under stress conditions. In our research, we observed a reduction in methylation and increase in hydroxymethylation in the region proximal to exon-8a under hypoxic conditions. This led us to investigate the role of epigenetic regulators in the alternative splicing of VEGFA. Our motif analysis identified the binding site of the epigenetic regulator CTCF on exon-8a. We validated CTCF binding through CTCF ChIP-qPCR and observed decrease in VEGFA-165a isoform when *CTCF* was depleted under hypoxic conditions. The results of our mechanistic studies provide evidence that CTCF mediates the inclusion of VEGFA-165 exon-8a under hypoxic condition.

In addition to performing their canonical function of monitoring splicing, splicing factors are capable of interacting with DNA-binding proteins such as transcription factors and epigenetic modifiers or can directly bind on DNA to regulate gene expression.[30,59] With this in mind, we hypothesized whether SRSF2 could be involved in regulating VEGFA-165 exon-8a inclusion by altering the methylation status under hypoxic conditions. To test this hypothesis, we conducted hMeDIP-qPCR following SRSF2 knockdown and observed increased hydroxymethylation at *VEGFA-165* exon-8a under normoxic conditions, which validated the involvement of SRSF2 in CTCF binding and inclusion of VEGFA-165 exon-8a. Additionally, our ChIP-qPCR results demonstrated a connection between SRSF2 and CTCF, as evidenced by increased CTCF and pol II enrichment in *SRSF2* knockdown cells relative to control cells. Our findings revealed the involvement of both SRSF2 and CTCF in orchestrating VEGFA-165 splicing. This study has identified the involvement of SRSF2 in regulation of the methylation status of the VEGFA-165 gene under hypoxic conditions, thus contributing to the existing understanding of the molecular mechanism involved in this biological process.

Of note, the findings of this study suggest a solid foundation for targeting the HIF1α-*miR222*-DNA hydroxymethylation-CTCF axis as a potential strategy to inhibit angiogenesis and combat breast cancer progression. Our research builds upon existing knowledge of VEGFA alternative splicing. Notably, our research demonstrates involvement of an miRNA in the mediation of VEGFA-165 alternative splicing and highlights an association between SRSF2 and CTCF in the regulation of VEGFA-165 splicing under hypoxic conditions in breast cancer.

Limitations of the study

One very obvious limitation of this study is its restriction to *in vitro* cell experiments. Also, there is lack of whole transcriptome data, presence of which could have strengthened the role of molecular players of this study in breast cancer progression. Another limitation is that this study only focused on two VEGFA

transcripts, whereas further research could explore the expression patterns and alternative splicing of other VEGFA transcripts under hypoxic condition. Future research must also elucidate the detailed mechanism behind SRSF2 regulating methylation status on VEGFA via DNMT3A. Moreover, it is important to note that *miR-222-3p* has multiple targets other than SRSF2, which could potentially play a role in regulating other cancer-related processes. This avenue of research warrants further exploration.

STAR★METHODS

Detailed methods are provided in the online version of this paper and include the following:

- KEY RESOURCES TABLE
- RESOURCE AVAILABILITY
  - Lead contact
  - Materials availability
  - Data and code availability
- EXPERIMENTAL MODEL DETAILS
  - Cell culture
  - Breast cancer sample collection
- METHOD DETAILS
  - Protein isolation from conditioned media
  - Western blotting
  - qRT-PCR
  - Semi-quantitative PCR
  - Molecular cloning
  - Minigene construct cloning
  - RNA interference
  - Luciferase dual reporter assays
  - miRNA mimic and inhibitor transfection
  - Chromatin immunoprecipitation (ChIP)
  - Methylated DNA immunoprecipitation (MeDIP) and hydroxymethylated DNA immunoprecipitation (hMeDIP)
  - Co-immunoprecipitation
  - Immunohistochemistry (IHC)
- QUANTIFICATION AND STATISTICAL ANALYSIS

SUPPLEMENTAL INFORMATION

Supplemental information can be found online at https://doi.org/10.1016/j.isci.2023.106804.

ACKNOWLEDGMENTS

The authors express their gratitude to all members of the Epigenetics and RNA Processing Lab for their valuable contributions and technical support. We thank Dr. Himanshu Kumar (IISER Bhopal, India) for the pMIR reporter plasmid. This research was funded by the Wellcome Trust/Department of Biotechnology (DBT) India Alliance Fellowship Grant IA/I/16/2/502719, awarded to S.S. This work is also supported by Science and Engineering Research Board (SERB) Grant (CRG/2021/004949, STR/2020/000093, and IPA/2021/000148). Additionally, P.Y. and A.P. were supported by Council of Scientific and Industrial Research fellowships. P.K. was supported by an Institute Postdoctoral Fellowship from the Indian Institute of Science Education and Research Bhopal. S.A.M. was also supported by the Indian Institute of Science Education and Research Bhopal.

AUTHOR CONTRIBUTIONS

Conceptualization, P.Y. and S.S.; Methodology, P.Y., P.K., and S.S.; Investigation, P.Y., P.K., and A.P.; Writing-Original Draft, P.Y., A.P., and S.S.; Writing-Review and Editing, S.A.M. and S.S.; Funding Acquisition, S.S.; Supervision, S.S.

DECLARATION OF INTERESTS

The authors have no conflict of interest to declare.

Received: February 13, 2023
Revised: March 21, 2023
Accepted: April 28, 2023
Published: May 4, 2023

REFERENCES

1. Sung, H., Ferlay, J., Siegel, R.L., Laversanne, M., Soerjomataram, I., Jemal, A., and Bray, F. (2021). Global cancer statistics 2020: GLOBOCAN estimates of incidence and mortality worldwide for 36 cancers in 185 countries. CA. Cancer J. Clin. *71*, 209–249. https://doi.org/10.3322/caac.21660.

2. Walsh, J.C., Lebedev, A., Aten, E., Madsen, K., Marciano, L., and Kolb, H.C. (2014). The clinical importance of assessing tumor hypoxia: relationship of tumor hypoxia to prognosis and therapeutic opportunities. Antioxid. Redox Signal. *21*, 1516–1554. https://doi.org/10.1089/ars.2013.5378.

3. Tan, Q., Wang, M., Yu, M., Zhang, J., Bristow, R.G., Hill, R.P., and Tannock, I.F. (2016). Role of autophagy as a survival mechanism for hypoxic cells in tumors. Neoplasia *18*, 347–355. https://doi.org/10.1016/j.neo.2016.04.003.

4. Hashimoto, T., and Shibasaki, F. (2015). Hypoxia-inducible factor as an angiogenic master switch. Front. Pediatr. *3*, 33. https://doi.org/10.3389/fped.2015.00033.

5. Al Tameemi, W., Dale, T.P., Al-Jumaily, R.M.K., and Forsyth, N.R. (2019). Hypoxia-modified cancer cell metabolism. Front. Cell Dev. Biol. *7*, 4. https://doi.org/10.3389/fcell.2019.00004.

6. Liao, D., and Johnson, R.S. (2007). Hypoxia: a key regulator of angiogenesis in cancer. Cancer Metastasis Rev. *26*, 281–290. https://doi.org/10.1007/s10555-007-9066-y.

7. Krock, B.L., Skuli, N., and Simon, M.C. (2011). Hypoxia-induced angiogenesis: good and evil. Genes Cancer *2*, 1117–1133. https://doi.org/10.1177/1947601911423654.

8. Mihalache, A., and Rogoveanu, I. (2014). Angiogenesis factors involved in the pathogenesis of colorectal cancer. Curr. Health Sci. J. *40*, 5–11. https://doi.org/10.12865/CHSJ.40.01.01.

9. Prager, G.W., Poettler, M., Unseld, M., and Zielinski, C.C. (2012). Angiogenesis in cancer: anti-VEGF escape mechanisms. Transl. Lung Cancer Res. *1*, 14–25. https://doi.org/10.3978/j.issn.2218-6751.2011.11.02.

10. Nowak, D.G., Woolard, J., Amin, E.M., Konopatskaya, O., Saleem, M.A., Churchill, A.J., Ladomery, M.R., Harper, S.J., and Bates, D.O. (2008). Expression of pro- and anti-angiogenic isoforms of VEGF is differentially regulated by splicing and growth factors. J. Cell Sci. *121*, 3487–3495. https://doi.org/10.1242/jcs.016410.

11. Zhu, H., and Zhang, S. (2018). Hypoxia inducible factor-1α/vascular endothelial growth factor signaling activation correlates with response to radiotherapy and its inhibition reduces hypoxia-induced angiogenesis in lung cancer. J Cell Biochem. *119*, 7707–7718. https://doi.org/10.1002/jcb.27120.

12. Rehn, M., Olsson, A., Reckzeh, K., Diffner, E., Carmeliet, P., Landberg, G., and Cammenga, J. (2011). Hypoxic induction of vascular endothelial growth factor regulates murine hematopoietic stem cell function in the low-oxygenic niche. Blood *118*, 1534–1543. https://doi.org/10.1182/blood-2011-01-332890.

13. Ahuja, N., Ashok, C., Natua, S., Pant, D., Cherian, A., Pandkar, M.R., Yadav, P., Vishnu, N.S.S., Mishra, J., Samaiya, A., and Shukla, S. (2020). Hypoxia-induced TGF-β–RBFOX2–ESRP1 axis regulates human MENA alternative splicing and promotes EMT in breast cancer. NAR Cancer *2*, zcaa021. https://doi.org/10.1093/narcan/zcaa021.

14. Liu, Y.R., Jiang, Y.Z., Xu, X.E., Hu, X., Yu, K.D., and Shao, Z.M. (2016). Comprehensive transcriptome profiling reveals multigene signatures in triple-negative breast cancer. Clin. Cancer Res. *22*, 1653–1662. https://doi.org/10.1158/1078-0432.CCR-15-1555.

15. Li, Q., Lai, H., Li, Y., Chen, B., Chen, S., Li, Y., Huang, Z., Meng, Z., Wang, P., Hu, Z., and Huang, S. (2021). RJunBase: a database of RNA splice junctions in human normal and cancerous tissues. Nucleic Acids Res. *49*, D201–D211. https://doi.org/10.1093/nar/gkaa1056.

16. Oltean, S., Gammons, M., Hulse, R., Hamdollah-Zadeh, M., Mavrou, A., Donaldson, L., Salmon, A.H., Harper, S.J., Ladomery, M.R., and Bates, D.O. (2012). SRPK1 inhibition in vivo: modulation of VEGF splicing and potential treatment for multiple diseases. Biochem. Soc. Trans. *40*, 831–835. https://doi.org/10.1042/BST20120051.

17. MacFarlane, L.-A., and Murphy, P.R. (2010). MicroRNA: biogenesis, function and role in cancer. Curr. Genomics *11*, 537–561. https://doi.org/10.2174/138920210793175895.

18. Kulshreshtha, R., Ferracin, M., Wojcik, S.E., Garzon, R., Alder, H., Agosto-Perez, F.J., Davuluri, R., Liu, C.-G., Croce, C.M., Negrini, M., et al. (2007). A MicroRNA signature of hypoxia. Mol. Cell Biol. *27*, 1859–1867. https://doi.org/10.1128/MCB.01395-06.

19. Camps, C., Saini, H.K., Mole, D.R., Choudhry, H., Reczko, M., Guerra-Assunção, J.A., Tian, Y.M., Buffa, F.M., Harris, A.L., Hatzigeorgiou, A.G., et al. (2014). Integrated analysis of microRNA and mRNA expression and association with HIF binding reveals the complexity of microRNA expression regulation under hypoxia. Mol. Cancer *13*, 1–21. https://doi.org/10.1186/1476-4598-13-28.

20. Kornblihtt, A.R. (2012). CTCF: from insulators to alternative splicing regulation. Cell Res. *22*, 450–452.

21. Lev Maor, G., Yearim, A., and Ast, G. (2015). The alternative role of DNA methylation in splicing regulation. Trends Genet. *31*, 274–280. https://doi.org/10.1016/j.tig.2015.03.002.

22. Alharbi, A.B., Schmitz, U., Bailey, C.G., and Rasko, J.E.J. (2021). CTCF as a regulator of alternative splicing: new tricks for an old player. Nucleic Acids Res. *49*, 7825–7838. https://doi.org/10.1093/nar/gkab520.

23. Marina, R.J., Sturgill, D., Bailly, M.A., Thenoz, M., Varma, G., Prigge, M.F., Nanan, K.K., Shukla, S., Haque, N., and Oberdoerffer, S. (2016). TET-catalyzed oxidation of intragenic 5-methylcytosine regulates CTCF-dependent alternative splicing. EMBO J. *35*, 335–355. https://doi.org/10.15252/embj.201593235.

24. López Soto, E.J., and Lipscombe, D. (2020). Cell-specific exon methylation and CTCF binding in neurons regulate calcium ion channel splicing and function. Elife *9*, e54879. https://doi.org/10.7554/eLife.54879.

25. Xiao, Y., and Yu, D. (2021). Tumor microenvironment as a therapeutic target in cancer. Pharmacol. Ther. *221*, 107753. https://doi.org/10.1016/j.pharmthera.2020.107753.

26. Shukla, S., Kavak, E., Gregory, M., Imashimizu, M., Shutinoski, B., Kashlev, M., Oberdoerffer, P., Sandberg, R., and Oberdoerffer, S. (2011). CTCF-promoted RNA polymerase II. Nature *479*, 74–79. https://doi.org/10.1038/nature10442.

27. Wang, Z., Li, K., Chen, W., Wang, X., Huang, Y., Wang, W., Wu, W., Cai, Z., and Huang, W. (2020). Modulation of SRSF2 expression reverses the exhaustion of TILs via the epigenetic regulation of immune checkpoint molecules. Cell. Mol. Life Sci. *77*, 3441–3452. https://doi.org/10.1007/s00018-019-03362-4.

28. Xiao, R., Chen, J.Y., Liang, Z., Luo, D., Chen, G., Lu, Z.J., Chen, Y., Zhou, B., Li, H., Du, X., et al. (2019). Pervasive chromatin-RNA binding protein interactions enable RNA-based regulation of transcription. Cell *178*, 107–121.e18. https://doi.org/10.1016/J.CELL.2019.06.001.

29. Pacini, C., and Koziol, M.J. (2018). Bioinformatics challenges and perspectives when studying the effect of epigenetic modifications on alternative splicing. Philos. Trans. R. Soc. Lond. B Biol. Sci. *373*, 20170073. https://doi.org/10.1098/rstb.2017.0073.

30. Zhang, J., Zhang, Y.Z., Jiang, J., and Duan, C.G. (2020). The crosstalk between epigenetic mechanisms and alternative RNA

processing regulation. Front. Genet. *11*, 998. https://doi.org/10.3389/fgene.2020.00998.

31. Olive, P.L., Aquino-Parsons, C., MacPhail, S.H., Liao, S.Y., Raleigh, J.A., Lerman, M.I., and Stanbridge, E.J. (2001). Carbonic anhydrase 9 as an endogenous marker for hypoxic cells in cervical cancer. Cancer Res. *61*, 8924–8929.

32. Waks, A.G., and Winer, E.P. (2019). Breast cancer treatment: a review. JAMA *321*, 288–300. https://doi.org/10.1001/jama.2018.19323.

33. Brahimi-Horn, M.C., Chiche, J., and Pouysségur, J. (2007). Hypoxia and cancer. J. Mol. Med. *85*, 1301–1307. https://doi.org/10.1007/s00109-007-0281-3.

34. Jing, X., Yang, F., Shao, C., Wei, K., Xie, M., Shen, H., and Shu, Y. (2019). Role of hypoxia in cancer therapy by regulating the tumor microenvironment. Mol. Cancer *18*, 157. https://doi.org/10.1186/s12943-019-1089-9.

35. Han, J., Li, J., Ho, J.C., Chia, G.S., Kato, H., Jha, S., Yang, H., Poellinger, L., and Lee, K.L. (2017). Hypoxia is a key driver of alternative splicing in human breast cancer cells. Sci. Rep. *7*, 4108. https://doi.org/10.1038/s41598-017-04333-0.

36. Farina, A.R., Cappabianca, L., Sebastiano, M., Zelli, V., Guadagni, S., and Mackay, A.R. (2020). Hypoxia-induced alternative splicing: the 11th hallmark of cancer. J. Exp. Clin. Cancer Res. *39*, 110. https://doi.org/10.1186/s13046-020-01616-9.

37. Liu, Z., Sun, L., Cai, Y., Shen, S., Zhang, T., Wang, N., Wu, G., Ma, W., Li, S.T., Suo, C., et al. (2021). Hypoxia-induced suppression of alternative splicing of MBD2 promotes breast cancer metastasis via activation of FZD1. Cancer Res. *81*, 1265–1278. https://doi.org/10.1158/0008-5472.CAN-20-2876.

38. Pant, D., Narayanan, S.P., Vijay, N., and Shukla, S. (2020). Hypoxia-induced changes in intragenic DNA methylation correlate with alternative splicing in breast cancer. J. Biosci. *45*, 3. https://doi.org/10.1007/s12038-019-9977-0.

39. Muz, B., de la Puente, P., Azab, F., and Azab, A.K. (2015). The role of hypoxia in cancer progression, angiogenesis, metastasis, and resistance to therapy. Hypoxia *3*, 83–92. https://doi.org/10.2147/HP.S93413.

40. Milani, M., and Harris, A.L. (2008). Targeting tumour hypoxia in breast cancer. Eur. J. Cancer *44*, 2766–2773. https://doi.org/10.1016/j.ejca.2008.09.025.

41. Ciarlillo, D., Celeste, C., Carmeliet, P., Boerboom, D., and Theoret, C. (2017). A hypoxia response element in the Vegfa promoter is required for basal Vegfa expression in skin and for optimal granulation tissue formation during wound healing in mice. PLoS One *12*, e0180586.

42. Dehghanian, F., Hojati, Z., and Kay, M. (2014). New insights into VEGF-A alternative splicing: key regulatory switching in the pathological process. Avicenna J. Med. Biotechnol. (AJMB) *6*, 192–199.

43. Biselli-Chicote, P.M., Oliveira, A.R., Pavarino, E.C., and Goloni-Bertollo, E.M. (2012). VEGF gene alternative splicing: pro- and anti-angiogenic isoforms in cancer. J. Cancer Res. Clin. Oncol. *138*, 363–370. https://doi.org/10.1007/s00432-011-1073-2.

44. Holmes, D.I., and Zachary, I. (2005). The vascular endothelial growth factor (VEGF) family: angiogenic factors in health and disease. Genome Biol. *6*, 209. https://doi.org/10.1186/gb-2005-6-2-209.

45. Peiris-Pagès, M. (2012). The role of VEGF 165b in pathophysiology. Cell Adh. Migr. *6*, 561–568. https://doi.org/10.4161/cam.22439.

46. Amin, E.M., Oltean, S., Hua, J., Gammons, M.V.R., Hamdollah-Zadeh, M., Welsh, G.I., Cheung, M.-K., Ni, L., Kase, S., Rennel, E.S., et al. (2011). WT1 mutants reveal SRPK1 to be a downstream angiogenesis target by altering VEGF splicing. Cancer Cell *20*, 768–780. https://doi.org/10.1016/j.ccr.2011.10.016.

47. Mavrou, A., Brakspear, K., Hamdollah-Zadeh, M., Damodaran, G., Babaei-Jadidi, R., Oxley, J., Gillatt, D.A., Ladomery, M.R., Harper, S.J., Bates, D.O., and Oltean, S. (2015). Serine-arginine protein kinase 1 (SRPK1) inhibition as a potential novel targeted therapeutic strategy in prostate cancer. Oncogene *34*, 4311–4319. https://doi.org/10.1038/onc.2014.360.

48. Peng, Y., and Croce, C.M. (2016). The role of microRNAs in human cancer. Signal Transduct. Target. Ther. *1*, 15004. https://doi.org/10.1038/sigtrans.2015.4.

49. Kong, F., Ran, W., Jiang, N., Li, S., Zhang, D., and Sun, D. (2019). Identification and characterization of differentially expressed miRNAs in HepG2 cells under normoxic and hypoxic conditions. RSC Adv. *9*, 16884–16891. https://doi.org/10.1039/c9ra01523j.

50. Boutz, P.L., Chawla, G., Stoilov, P., and Black, D.L. (2007). MicroRNAs regulate the expression of the alternative splicing factor nPTB during muscle development. Genes Dev. *21*, 71–84. https://doi.org/10.1101/gad.1500707.

51. Yao, P., Wu, J., Lindner, D., and Fox, P.L. (2017). Interplay between miR-574-3p and hnRNP L regulates VEGFA mRNA translation and tumorigenesis. Nucleic Acids Res. *45*, 7950–7964. https://doi.org/10.1093/nar/gkx440.

52. Cuzziol, C.I., Castanhole-Nunes, M.M.U., Pavarino, É.C., and Goloni-Bertollo, E.M. (2020). MicroRNAs as regulators of VEGFA and NFE2L2 in cancer. Gene *759*, 144994. https://doi.org/10.1016/j.gene.2020.144994.

53. Semenza, G.L. (2012). Hypoxia-inducible factors in physiology and medicine. Cell *148*, 399–408. https://doi.org/10.1016/j.cell.2012.01.021.

54. Luco, R.F., Allo, M., Schor, I.E., Kornblihtt, A.R., and Misteli, T. (2011). Epigenetics in alternative pre-mRNA splicing. Cell *144*, 16–26. https://doi.org/10.1016/j.cell.2010.11.056.

55. Kim, S., Kim, H., Fong, N., Erickson, B., and Bentley, D.L. (2011). Pre-mRNA splicing is a determinant of histone H3K36 methylation. Proc. Natl. Acad. Sci. USA *108*, 13564–13569. https://doi.org/10.1073/pnas.1109475108.

56. de Almeida, S.F., Grosso, A.R., Koch, F., Fenouil, R., Carvalho, S., Andrade, J., Levezinho, H., Gut, M., Eick, D., Gut, I., et al. (2011). Splicing enhances recruitment of methyltransferase HYPB/Setd2 and methylation of histone H3 Lys36. Nat. Struct. Mol. Biol. *18*, 977–983. https://doi.org/10.1038/nsmb.2123.

57. Zhou, H.L., Hinman, M.N., Barron, V.A., Geng, C., Zhou, G., Luo, G., Siegel, R.E., and Lou, H. (2011). Hu proteins regulate alternative splicing by inducing localized histone hyperacetylation in an RNA-dependent manner. Proc. Natl. Acad. Sci. USA *108*, E627–E635. https://doi.org/10.1073/pnas.1103344108.

58. Zhu, L.-Y., Zhu, Y.-R., Dai, D.-J., Wang, X., and Jin, H.-C. (2018). Epigenetic regulation of alternative splicing. Am. J. Cancer Res. *8*, 2346–2358.

59. Tanis, S.E.J., Jansen Pascal, W.T.C., Zhou, H., van Heeringen, S.J., Vermeulen, M., Kretz, M., and Mulder, K.W. (2018). Splicing and chromatin factors jointly regulate epidermal differentiation. Cell Rep. *25*, 1292–1303.e5. https://doi.org/10.1016/j.celrep.2018.10.017.

STAR★METHODS

KEY RESOURCES TABLE

REAGENT or RESOURCE	SOURCE	IDENTIFIER
Antibodies		
SRSF2	Abcam	Cat# Ab28428; Lot No. GR154517-43; RRID:AB_777854
VEGFA-165a	Sigma	Cat# SAB4200815; Lot No. 059M5885V
VEGFA-165b	Merck	Cat# MABC595; Lot No. 3723491
CAIX	Abcam	Cat# ab184006; Lot No. GR173128-25
CTCF	CST	Cat# 3418S; Lot No. 4; RRID:AB_2086791
HIF1α	CST	Cat# 14179S; Lot No. 3; RRID:AB_2622225
α-CTD	CST	Cat# 2629S; Lot No. 3,
α-Tubulin	Abcam	Cat# Ab7291; RRID:AB_2241126
DNMT3A	CST	Cat# 32578S; Lot No.10; RRID:AB_2799025
Anti-Flag	Novus Biologicals	Cat# NBP1-06712SS; RRID:AB_1625981
5-Methylcytosine (5-mC)	CST	Cat# 28692S; Lot No. 2; RRID:AB_2798962
5-Hydroxymethylcytosine (5-hmC)	CST	Cat# 51660S; Lot No. 2; RRID:AB_2799398
Alexa-Fluor 680 anti-rat IgG	Invitrogen	Cat# A21096; Lot No. B-6
Alexa-Fluor 800 anti-mouse IgG	Invitrogen	Cat# A32730; Lot No. SC243837
Alexa-Fluor 680 anti-rabbit IgG	Invitrogen	Cat# A32734; Lot No. RJ243414
Normal Rabbit IgG	CST	Cat# 2729S; Lot No. 2010149; RRID:AB_1031062
Normal Mouse IgG	CST	Cat# 5415S; Lot No. 8; RRID:AB_10829607
Bacterial and virus strains		
E.coli stbl3 cells	ThermoFisher Scientific	Cat# C737303
Biological samples		
Breast cancer patients tissue sections; See Table S1	Bansal Hospital	N/A
Chemicals, peptides, and recombinant proteins		
Lipofectamine 2000	ThermoFisher Scientific	Cat# 11668019
SYBR Green Master Mix	Promega	Cat# A6101
PrimeScript cDNA synthesis kit	TaKaRa	Cat# 6110A
Protein G Dynabeads	Thermo Fisher Scientific	Cat# 10004D, Lot No. 0078227
TaqMan™ Fast Advanced Master Mix	Thermo Fischer Scientific	Cat# 4444557
TaqMan™ miRNA Reverse Transcription kit	Thermo Fischer Scientific	Cat# 4366596
RNase A	Thermo Fischer Scientific	Cat# 12091021
DMEM medium	Invitrogen	Cat# 12800017, Lot No. 2248833
RPMI medium	Invitrogen	Cat# 23400021, Lot No. 2144859
Fetal Bovine Serum	Sigma	Cat# F7524, Lot No. BCBX8466
Penicillin and Streptomycin	Invitrogen	Cat# 15140122, Lot No. 2321120
Polybrene	Sigma	Cat# H9268, Lot No. SLBH5907V
Puromycin	Sigma	Cat# P9620, Lot No. 034M4008V
TRIzol	Invitrogen	Cat# 15596018, Lot No. 260712
Fluoroshield	Sigma	Cat# F6182
Dream Taq polymerase	Thermo Fisher Scientific	Cat# EP0702
Phusion DNA polymerase	Thermo Fisher Scientific	Cat# M0530S

(*Continued on next page*)

Continued

REAGENT or RESOURCE	SOURCE	IDENTIFIER
L-Glutamine	Invitrogen	Cat# 25030081, Lot No. 1917006
Bobcat339	Sigma	Cat# SML2611
Proteinase K	Thermo Fischer Scientific	Cat# 25530049
Critical commercial assays		
QIAquick Gel extraction Kit	Qiagen	Cat# 28706
QIAquick PCR purification Kit	Qiagen	Cat# 28106
Dual-Luciferase Reporter Assay System	Promega	Cat# E1910
Plasmid mini kit	Qiagen	Cat# 27106
TaqMan™ miRNA assays (miRNA-222-3p)	Applied Biosystems	Assay ID 002276, Cat# 4427975
TaqMan™ miRNA assays (U6)	Applied Biosystems	Assay ID 001973, Cat# 4427975
Experimental models: Cell lines		
HEK293T	ATCC	Cat# CRL-3216
MCF7	ATCC	Cat# HTB -22
HCC1806	ATCC	Cat# CRL-2335
Oligonucleotides		
Primers for RT-PCR and qRT-PCR, See Table S2	This paper	N/A
Primers for Cloning, See Table S3	This paper	N/A
miRNA inhibitor negative control	Thermo Fisher Scientific	Cat# 4464076
miRNA mimic negative control	Thermo Fisher Scientific	Cat# 4464058
miRNA-222-3p Inhibitor	Thermo Fisher Scientific	Cat# 4464084
miRNA-222-3p mimic	Thermo Fisher Scientific	Cat# 4464066
shRNA sequences, See Table S4	Sigma shRNA library	N/A
Deposited data		
HTA 2.0 microarray (MCF7 cells)	PMID: 33089214 [13]	GEO: GSE147516
HTA 2.0 microarray (Breast cancer patients)	PMID: 26813360.[14]	GEO: GSE76250
Software and algorithms		
Image J	NIH	https://imagej.nih.gov/ij/
SFmap	BioTools	https://bio.tools/sfmap
Prism	Graphpad	https://www.graphpad.com/scientificsoftware/prism/
STRING	PMID: 25352553	https://string-db.org/
PrimerQuest Tool	IDT	https://www.idtdna.com
Target Scan	PMID: 17612493	https://www.targetscan.org/
CIS-BP	PMID: 25215497	http://cisbp.ccbr.utoronto.ca
Eukaryotic Promoter Database	Swiss Institute of Bioinformatics	https://epd.vital-it.ch/
ChIP-Atlas	PMID: 35325188	https://chip-atlas.org
RJunBase software	(Li et al., 2021)[15]	http://www.rjunbase.org/

RESOURCE AVAILABILITY

Lead contact

Further information and requests for resources and reagents should be directed to and will be fulfilled by the lead contact, Sanjeev Shukla (sanjeevs@iiserb.ac.in).

Materials availability

This Study did not generate new unique reagents.

Data and code availability

- This paper analyses existing, publicly available data. These accession numbers for the datasets are listed in the key resources table. All data reported in this paper will be shared by the lead contact upon request
- This paper does not report original code
- Any additional information required to reanalyse the data reported in this paper is available from the lead contact upon request.

EXPERIMENTAL MODEL DETAILS

Cell culture

The MCF7 and HCC1806 human breast cancer cell and HEK293T cells were obtained from the American Type Culture Collection (ATCC). These cell lines were grown in media recommended by ATCC, which included DMEM for MCF7 and HEK293T and RPMI for HCC1806. Both media were supplemented with 10% fetal bovine serum (Sigma, F7524), 100 units/ml of penicillin and streptomycin (Invitrogen, 15140122), and 2 mmol/l L-glutamine (Invitrogen, 25030081) All cell lines were maintained in a humidified atmosphere at 37°C and 5% CO_2 incubator. To stimulate hypoxic conditions, cells were placed in a Ruskinn INVIVO2 400 hypoxia chamber and exposed to a gas mixture containing 1% O_2 and 5% CO_2 for 24 hours. Bobcat339 dissolved in DMSO (90 μM) (Sigma, SIML2611) was added to the media to inhibit TET activity. The cell lines used in the study were authenticated from a national cell repository facility by short tandem repeats (STR) profiling and were routinely tested for mycoplasma contamination using PCR based method.

Breast cancer sample collection

The study utilized breast tumor paraffin-embedded tissue samples obtained from Bansal hospital in Bhopal, India. These samples were placed on poly-L-lysine coated slides. Patient samples details are provided in Table S1. The use of these tissue samples was approved by the Institute Ethics Committee of the Indian Institute of Science Education and Research in Bhopal, India.

METHOD DETAILS

Protein isolation from conditioned media

For protein precipitation from conditioned media, 1 ml of 20% Trichloroacetic acid was added to 1 ml of conditioned media. The solution was incubated on ice for 15 minutes. Microcentrifugation was performed at 14,000 rpm for 5 minutes at 4°C. Supernatant was removed and pellet was washed twice with 500 μl of ice-cold acetone, with subsequent centrifugation at 14,000 rpm for 5 minutes at 4°C. The pellet was air dried and dissolved in 1X laemmli buffer. Protein samples were heated at 95°C before proceeding for western blotting.

Western blotting

The breast cancer cells were lysed using a urea-based buffer containing 8 M urea, 2 M thiourea, 2% CHAPS, and 1% DTT, as well as 1× PIC (leupeptin 10–100 μM, pepstatin 1 μM, 1–10 mM EDTA, <1 mM AEBSF). The cell debris was removed by centrifuging the lysate at 16,000 ×g at 4°C, and the protein concentration was determined using the Bradford assay. Equal amounts of total protein were separated by 12-15% SDS-PAGE and transferred to a PVDF membrane from Millipore. Following this, the membrane was blocked with 10% skimmed milk in TBST for 1 hour at room temperature, and the primary antibodies were incubated overnight at 4°C. The membrane was then washed twice with TBST containing 0.05% Tween 20 and incubated with the secondary antibody for 1 hour at room temperature. The bands were quantified using GelQuant software. The antibodies used were Anti-SRSF2 (Abcam, ab28428, 1:1000), HIF1α (CST, 14179S, 1:1000), CTCF (CST, 3418S, 1:1000), GAPDH (CST, 5174S, 1:1000), Anti-VEGF 165b (Merck, MABC595, 1:500), Anti-VEGF 165a (Abcam, Ab69479, 1:500), and DNMT3A (CST, 32578S, 1:1000). Additional information regarding the antibodies can be found in key resources table.

qRT-PCR

The total RNA was extracted from breast cancer cells using TRIzol reagent (Invitrogen, Cat# 15596018, Lot No. 260712), according to the manufacturer's protocol. The concentration of the extracted RNA was measured using a Biospectrophotometer (Eppendorf). Two micrograms of the total RNA was reverse-transcribed using the PrimeScript RT reagent kit (Takara, Cat# 6110A) with Oligo dT primers. Twenty

nanograms of the cDNA was used as the template for PCR amplification using SYBR Green (Promega) in a Light Cycler 480 II (Roche). The expression of *miR-222-3p* was evaluated using the TaqMan Universal PCR master mix (Thermo Fischer Scientific) and the TaqMan miRNA Assay Kit (Thermo Fischer Scientific). The average cycle threshold values were obtained from biological triplicates. The samples' mRNA and miRNA expression was normalized to RPS16 and U6, respectively using the formula 2^ (Ct control - Ct target). Additional information regarding the reagents can be found in key resources table. The significance between the two different groups was determined using a Student's t-test, with a p value of less than 0.05 considered statistically significant. The primers used in the experiment are listed in Table S2.

Semi-quantitative PCR

The TRIzol reagent was used to lyse the cells, RNA extraction was performed according to the manufacturer's instructions. The resulting RNA was resuspended in 30 μl nuclease free water and concentration was determined using Biospectrophotometer (Eppendorf). To generate cDNA, 2 μg total RNA was reverse transcribed using PrimeScipt 1st strand synthesis kit (TaKaRa, 6110A), according to the manufacturer's instructions. The resulting cDNA was subjected to PCR using Dream Taq polymerase (Thermo Fisher Scientific, EP0702) and flanking primers for VEGFA-165a, VEGFA-165b and 18s rRNA. After 35 cycles of amplification, PCR products were separated on 2% agarose gel. Gel extraction was used to isolate fragments specific for VEGFA-165a and VEGFA-165b, which were then sent for Sanger sequencing to confirm their sequences. The primers used in the experiment are listed in Table S2.

Molecular cloning

The SRSF2 gene was cloned using the pCMV-3Tag-1a overexpression plasmid from Agilent (240195) and MCF7 cDNA. The amplification was carried out using Phusion DNA polymerase, and the SRSF2 overexpression fragment was inserted between the EcoRI forward and BamHI reverse sites. To investigate the role of transcription factors in regulating SRSF2 expression, a deletion construct of the SRSF2 promoter was created by retrieving the promoter sequence from −2000bp to +100bp of the transcription start site from the Eukaryotic Promoter Database (https://epd.vital-it.ch/) and amplified using PCR and Phusion DNA polymerase. The amplified fragment was cloned into the pGL3-Basic expression vector (Promega, E1751) between the Kpn1 forward and XhoI reverse sites.

To clone the SRSF2 3'UTR containing *miR-222-3p* binding sites (wild type and mutant), approximately 100 bp long 3'UTR forward and reverse strands were commercially synthesized. The oligonucleotides were annealed by incubation for 4 minutes at 95°C. The microtube was allowed to cool gradually at room temperature, and the resulting duplex oligonucleotide was cloned in a pMIR reporter plasmid. All plasmids were verified by Sanger sequencing. The primers used for the cloning are listed in Table S3.

Minigene construct cloning

Phusion DNA polymerase was used to amplify fragments consisting of VEGFA exon-7, intron-7, and exon-8 region in a PCR reaction of 35 cycles, for the purpose of creating a minigene construct. Three different fragments were amplified and ligated by overlapping PCR. First fragment was amplified using VEGFA exon-7 forward and exon-8a reverse primers. Second fragment was amplified using VEGFA exon-8a forward and exon-8b reverse primers. Third fragment was amplified using VEGFA exon-8b/eGFP overhangs forward and eGFP reverse using eGFP-N1 plasmid as template. The fragments were joined using an overlapping extension PCR technique, where the first 15 cycles were performed without primers and the remaining 20 cycles with flanking primers. PCR products were taken in equimolar amounts for overlapping PCR with calculation performed using NEBiocalculator. The resulting amplified fragment was then verified by gel electrophoresis on a 1.5% gel and digested using EcoR1 and BamH1 enzymes (Takara Bio-USA Inc.) in a total 30 μl reaction volume, which was kept for 2 hours in a water bath at 37°C. The digested products were then PCR purified. Ligation of the mCherry-N1 vector and insert was performed at a ratio of 1:3 using T4 endonuclease ligase in a total 20 μl reaction and kept for 1 hour at 16°C. The transformation was performed using *E. coli* Stbl3 competent cells, with the pmCherry-N1 vector used as the positive control. Positive clones were confirmed using specific primers in a colony PCR consisting of 35 cycles. Restriction digestion with EcoR1 and BamH1 enzymes and sequencing were also used to verify positive clones. Transfection with the minigene construct was done in MCF7 cells using lipofectamine 2000 transfection reagent. Imaging was done after 24 hours of transfection. To prepare the cells for confocal imaging, they were washed twice with ice-cold PBS and then treated with 4% formaldehyde solution prepared in PBS. The cells were incubated at room temperature for 10 minutes, followed by two more PBS washes. Next, DAPI was added

to the cell and they were incubated for 5 minutes at room temperature. The cells were then given two PBS washes and finally, mounted on coverslip using Fluoroshield mounting media (Sigma). Slides were analyzed using an Olympus FV3000 confocal laser scanning microscope with a 60× Plan Apo N objective (oil, 1.42 NA). Details for primers used in minigene cloning are given in Table S3.

RNA interference

Small hairpin RNAs (shRNA) targeting genes SRSF2, CTCF, DNMT3A, and HIF1α were obtained from Sigma's Mission Human Genome shRNA Library. Lentivirus containing shRNA plasmid were generated by transfecting HEK293T cells with Δ8.9 and VSVG plasmid along with the required shRNA containing plasmid in 1:0.5:2 ratio using polyethylenimine (PEI). The MCF7 and HCC1806 cell lines were seeded in six-well culture plates, and transduced with a lentivirus solution containing the specific shRNA and polybrene. The cells were then spun at 2200 rpm for 90 minutes, and selected using 1 μg/ml puromycin for 3 days. The cells were then maintained in a humidified incubator at 37°C with 5% CO_2. The knockdown of the targeted genes was confirmed by western blotting, and the cells were then used for downstream experiments. Additional information regarding the reagents used are added in key resources table. The shRNA sequences used are provided in Table S4.

Luciferase dual reporter assays

Dual luciferase assay was performed using SRSF2 promoter Firefly luciferase construct, and SRSF2 3′UTR wild-type/mutant Firefly luciferase constructs. For the assay, HCC1806 and MCF7 cells were seeded in 24-well plates and allowed to grow for 24 hours. Following this, Lipofectamine 2000 (Invitrogen) was used to co-transfect the cells with 200 ng of different Firefly luciferase constructs and 50 ng of pRL-TK Renilla luciferase plasmid (Promega, E2231). The cells were then exposed to normoxia/hypoxic treatment for an additional 24 hours and lysed in passive lysis buffer (Promega). The activity of the luciferase was measured using the GloMax-Multi Detection System (Promega). The results were analyzed by normalizing the firefly luciferase activity with the Renilla luciferase activity. The data is presented as the mean ± SD of biological triplicates.

miRNA mimic and inhibitor transfection

MCF7 and HCC1806 cells were seeded in 6 well culture plates 24 hours before transfection. Synthetic *miR-222-3p* mimic and inhibitor, as well as their scrambled negative controls (90 pmoles) purchased from Ambion, Thermo Fisher Scientific, were transfected using lipofectamine 2000 and optiMEM media according to the manufacturer's instructions. Following 24 hours of transfection, the media was substituted with the fresh media and the cells were exposed to additional treatment. After another 24 hours of either normoxia or hypoxia treatment, the cells were harvested for RNA and protein. Additional information regarding the reagents used are added in key resources table.

Chromatin immunoprecipitation (ChIP)

Chromatin immunoprecipitation was performed to evaluate the binding of transcription factors and DNA binding proteins on chromatin. Initially, approximately 20 million cells were lysed, and the resulting lysate was sonicated to generate chromatin fragment with lengths ranging from 200–500 bp. 1/20 of 20% Triton X-100 was added to the sonicated lysate and centrifugation was performed at 16,000 × g for 10 minutes at 4°C to pellet debris. 30 μl of chromatin was de-crosslinked by incubating it with RNAse for 30 minutes at 37°C followed by the addition of Proteinase K at 65°C for 2 hours. DNA was purified using Qiagen PCR purification kit and elution was done in 30 μl elution buffer. DNA concentration was determined using Biospectrophotometer (Eppendorf). To immunoprecipitated chromatin, 25 μg of sonicated chromatin was diluted with 20% Triton X-100 containing LB3 and incubated overnight at 4°C with 2–3 μg concomitant antibodies. The next day, 30 μl of magnetic beads were added per sample, and the mixture was incubated at 4°C for 2 hours. The microcentrifuge tubes were then spun down and kept on magnetic stand to separate the beads. Consequent washes with low salt, high salt, LiCl and TE buffer were given using magnetic stand. Elution was done with 150 μl elution buffer at 65°C overnight with shaking at 900 rpm. Centrifugation at 16,000 × g for 1 minute was done to pellet down beads. Supernatant was transferred to new centrifuge tube and 1 μl RNAse A (1 mg/ml) was added and incubation at 37°C for 30 minutes was performed. Same was done with the input samples. Next, 1 μl Proteinase K (20 mg/ml) was added and incubation at 65°C was performed overnight for de-crosslinking. The immunoprecipitated protein–DNA complexes and 5% input were analyzed by qRT-PCR with SYBR Green master mix (Promega) in triplicate using specific primers flanking the predicted binding sites. IP values were normalized to input using the following

formula: 2^ (Ct input − Ct immunoprecipitation). Resultant values were subsequently normalized to IgG control IP values. All the ChIP experiments were performed at least thrice. The significance between different groups was determined using a Student's t-test, with a P-value less than 0.05 considered statistically significant. The following antibodies were used: anti-CTCF, anti-HIF1α, anti-CTD (CST, 2629S), normal rabbit IgG (CST, 2729S), and normal mouse IgG (CST, 5415S).

Methylated DNA immunoprecipitation (MeDIP) and hydroxymethylated DNA immunoprecipitation (hMeDIP)

The genomic DNA of MCF7 and HCC1806 cells was extracted using genomic DNA isolation kit from Sigma (G1N350) according to the manufacturer's instructions. Genomic DNA was sonicated to get DNA fragments between size 250–500 bp. Sonicated DNA was denatured by incubating at 95°C for 10 minutes. 3 μg of sonicated DNA was incubated with 1 μg anti-5-Methylcytosine (CST, 28692S) or anti-5-hydroxymethylcytosine (CST, 51660S) antibodies along with normal rabbit IgG or normal mouse IgG at 4°C overnight. 30 μl magnetic beads were added and incubated for 2 hours at 4°C. The beads were washed thrice with 500 μl MeDIP buffer at 4°C for 5 minutes and eluted in 150 μl elution buffer with proteinase K treatment, overnight at 65°C at 900 rpm. PCR purification was performed using Qiagen PCR purification kit. The immunoprecipitated fractions and 5% input were analyzed using quantitative real-time PCR using the SYBR Green Master Mix (Promega, A6002, lot no. 0000385100) and specific primers (listed in Table S2). The experiments were performed at least in triplicate. IP values were normalized to input using the formula: 2^ (Ct_input − Ct_immunoprecipitation). The significance between the two different groups was determined using a Student's t-test, with a p value of less than 0.05 considered statistically significant.

Co-immunoprecipitation

The interaction between DNMT3A and SRSF2 was analysed using a co-immunoprecipitation (co-IP) assay. MCF7 cells were harvested by trypsinization after being washed with PBS. The cells were then lysed with a lysis buffer containing 10 mM Tris (pH 7.5), 150 mM NaCl, 0.5 mM EDTA, 0.5% NP-40, and a protease inhibitor cocktail. To conduct the assay,1 mg of protein lysate was incubated with 2 μg of DNMT3A-specific antibodies and normal rabbit IgG for 4 hours at 4°C. Following this, 25 μl Protein-G Dynabeads were added to the immunoprecipitated lysate and further incubated for 2 hours at 4°C. The beads were subsequently washed thrice with 500 μl of the lysis buffer and boiled in 2X Laemmli buffer for 5 minutes at 95°C. The eluted proteins were analyzed using immunoblotting with anti-DNMT3A and anti-SRSF2 antibodies.

Immunohistochemistry (IHC)

Human breast cancer tissue samples were obtained from Bansal Hospital in Bhopal, India, and processed for IHC analysis using the Vectastain ABC Elite kit (Vector Laboratories, Burlingame, CA, USA). The tissues were formalin fixed, paraffin-embedded, and sliced into thin sections for subsequent staining. To prepare the sections for histological analysis, they were fixed on a heat block for 5 hours, deparaffinized, and rehydrated according to standard procedure. Antigen retrieval was performed by heating sections in 10 mM sodium citrate buffer (pH 6) for 13 minutes, the sections were kept at room temperature for gradual cooling. The endogenous peroxidase was quenched with a 1:10 dilution of 3% hydrogen peroxidase in methanol. 3% bovine serum albumin was used to block non-specific binding, and primary antibodies were incubated overnight at 4°C with the sections. The DAB chromogenic method (Sigma) was used for visualization, along with Harris' hematoxylin counterstaining (Merck). The primary antibodies used were against CAIX (1:50), SRSF2 (1:50), VEGFA-165a (1:25) and VEGFA-165b (1:25). Images were captured using the Thermo Scientific™ Invitrogen™ EVOS™ FL Auto 2 Imaging System at 40× magnification. Informed consent was obtained from all patients, and details are provided in Table S1.

QUANTIFICATION AND STATISTICAL ANALYSIS

All statistical analyses were conducted using GraphPad Prism 8 software (GraphPad Software, La Jolla, USA). Unless otherwise stated, all data are represented as mean ±SD analyzed using an unpaired two-tailed Student's t-test. Statistical methods for each analysis are described in figure legends. Independently performed biological replicates are indicated as dots in the bar graphs. Statistical significance is denoted as follows: *$p < 0.05$, **$p < 0.01$, ***$p < 0.001$, and ****$p < 0.0001$, while a lack of significance is represented by "ns" for $p > 0.05$.